Popular Summary: Much of what we currently know about the large scale variability of and trends in the global sea ice cover has been based on data provided by satellite passive microwave sensors. While large changes in the sea ice cover have been observed during the satellite era, uncertainties in the trends have been difficult to assess because of the lack of adequate validation data. With the launched of the Advanced Microwave Scanning Radiometer in May 2002 on board the EOS-Aqua satellite (referred to as "AMSR-E"), however, ability to assess the accuracy of historical data has improved considerably because of much better resolution and hence accuracy in the former. This study shows that during the overlap period from June 2002 to 2006, highly consistent ice concentration maps can be derived from both AMSR-E and SSM/I data if the two data sets are inter-calibrated and the same algorithm is used to derive geophysical parameters. The ice extent estimates from SSM/I data, however, are consistently higher than those from AMSR-E while the ice area estimates are almost identical. This is shown to be caused by more precise definition of the ice edge provided by AMSR-E compared to that of SSM/I due to better resolution. Since the data record of AMSR-E is too short at less then 5 years, change studies using AMSR-E data can only be done if the latter are combined with historical satellite data. We show that this can be done successfully for ice area without any normalization of the data. It can also be done with ice extent through proper normalization of SSM/I and SMMR data. The estimates for trends in ice extent and ice area from the resulting data sets are shown to be consistent with those derived from historical data. The higher accuracy of the AMSR-E data, however, provides improved reliability in the data set and greater confidence in the trend values.

Significant Findings: With higher resolution and improved accuracy, AMSR-E data provide a good baseline for sea ice cover studies and can be used to validate geophysical parameters derived from historical data. Comparative studies of AMSR-E and SSM/I data during the 5 year period of overlap shows basically good consistency in the derived geophysical products. The most serious source of discrepancy is in the characterization of the ice edge and marginal ice zone in which AMSR-E clearly show improvements because of higher resolution. Thus SSM/I shows an ice edge location that is on the average about 6 to 12 km further away from the ice pack than AMSR-E data. Biases if uncorrected contribute to errors in the estimates of trends in extents by as much as 0.62%/decade in the Arctic and 0.26%/decade in the Antarctic. The biases in the trends of ice area are less with the error in the trend being at 0.30%/decade in the Arctic and 0.05%/decade in the Antarctic. Using time series data from SMMR, SSM/I and AMSR-E (starting June 2002) and after correcting for the aforementioned bias, the results of our regression analysis for period from November 1978 to December 2006 yielded trends in extent and area of sea ice in the Arctic region are -3.4 ± 0.2 and -4.0 ± 0.2 % per decade, respectively. The corresponding values for the Antarctic region are 0.9 ± 0.2 and 1.7 ± 0.3 % per decade. These trends are basically the same as those derived using SMMR and SSM/I data only, but with AMSR-E providing more accurate values for the last few years of the data set, the degree of confidence in the trend is higher with the latter included. With time, the data from AMSR-E and similar instruments will increase the reliability of the trend values.

Title: Trends in the Sea Ice Cover using Enhanced and Compatible AMSR-E, SSM/I and SMMR Data

Authors: Josefino C. Comiso, Cryospheric Sciences Branch, Code 614.1, NASA Goddard Space Flight Center, Greenbelt, MD 20771, email: Josefino.c.comiso@NASA.gov, and Fumihiko Nishio, Center for Environmental Remote Sensing, Chiba University 1-33 Yayoi-cho, Chiba City, Japan, email: fnishio@cr.chiba-u.ac.jp

Journal: JGR-Oceans - for the special section on "Large Scale Characteristics of the Sea Ice Cover from AMSR-E and other Satellite Sensors"

Abstract: Arguably, the most remarkable manifestation of change in the polar regions is the rapid decline (of about -10 %/decade) in the Arctic perennial ice cover. Changes in the global sea ice cover, however, are more modest, being slightly positive in the Southern Hemisphere and slightly negative in the Northern Hemisphere, the significance of which has not been adequately assessed because of unknown errors in the satellite historical data. We take advantage of the recent and more accurate AMSR-E data to evaluate the true seasonal and interannual variability of the sea ice cover, assess the accuracy of historical data, and determine the real trend. Consistently derived ice concentrations from AMSR-E, SSM/I, and SMMR data were analyzed and a slight bias is observed between AMSR-E and SSM/I data mainly because of differences in resolution. Analysis of the combine SMMR, SSM/I and AMSR-E data set, with the bias corrected, shows that the trends in extent and area of sea ice in the Arctic region is -3.4 ± 0.2 and -4.0 ± 0.2 % per decade, respectively, while the corresponding values for the Antarctic region is 0.9 ± 0.2 and 1.7 ± 0.3 % per decade. The higher resolution of the AMSR-E provides an improved determination of the location of the ice edge while the SSM/I data show an ice edge about 6 to 12 km further away from the ice pack. Although the current record of AMSR-E is less than 5 years, the data can be utilized in combination with historical data for more accurate determination of the variability and trends in the ice cover.

Trends in the Sea Ice Cover using Enhanced and Compatible AMSR-E, SSM/I and SMMR Data

Josefino C. Comiso
Cryospheric Sciences Branch, Code 614.1, NASA Goddard Space Flight Center
Greenbelt, MD 20771, email: Josefino.c.comiso@NASA.gov

Fumihiko Nishio
Center for Environmental Remote Sensing, Chiba University
1-33 Yayoi-cho, Chiba City, Japan, email: fnishio@cr.chiba-u.ac.jp

Submitted to JGR-Oceans
Special Section on "Large Scale Characteristics of the Sea Ice Cover from AMSR-E and other Satellite Sensors"

Running Title: Trends in the Sea Ice Cover from Space
Keywords: Sea ice, Arctic and Antarctic, Climate Change, Satellite Remote Sensing

Abstract

Arguably, the most remarkable manifestation of change in the polar regions is the rapid decline (of about -10 %/decade) in the Arctic perennial ice cover. Changes in the global sea ice cover, however, are more modest, being slightly positive in the Southern Hemisphere and slightly negative in the Northern Hemisphere, the significance of which has not been adequately assessed because of unknown errors in the satellite historical data. We take advantage of the recent and more accurate AMSR-E data to evaluate the true seasonal and interannual variability of the sea ice cover, assess the accuracy of historical data, and determine the real trend. Consistently derived ice concentrations from AMSR-E, SSM/I, and SMMR data were analyzed and a slight bias is observed between AMSR-E and SSM/I data mainly because of differences in resolution. Analysis of the combine SMMR, SSM/I and AMSR-E data set, with the bias corrected, shows that the trends in extent and area of sea ice in the Arctic region is -3.4 ± 0.2 and -4.0 ± 0.2 % per decade, respectively, while the corresponding values for the Antarctic region is 0.9 ± 0.2 and 1.7 ± 0.3 % per decade. The higher resolution of the AMSR-E provides an improved determination of the location of the ice edge while the SSM/I data show an ice edge about 6 to 12 km further away from the ice pack. Although the current record of AMSR-E is less than 5 years, the data can be utilized in combination with historical data for more accurate determination of the variability and trends in the ice cover.

1. Introduction

Much of what we currently know about the large scale variability of the global sea ice cover has been based on data provided by satellite passive microwave sensors (Parkinson et al., 1999; Bjorgo et al., 1999; Zwally, 2002). This capability for studying the sea ice cover has recently been improved considerably with the launched of the Advanced Microwave Scanning Radiometer in May 2002 on board the EOS-Aqua satellite (referred to as "AMSR-E") and in December 2002 on board Midori-2 (called "AMSR"). In this paper, we will use results primarily from AMSR-E which is the only sensor of the two that is currently providing data because of the unexpected power failure in the Midori-2 satellite after 9 months of operation. The improvements of AMSR-E over the Special Scanning Microwave Imager (SSM/I), which has been the primary source of data since July 1987, include higher resolution at all frequencies, wider spectral range, and less radiometer noise. In particular, AMSR-E has integrated field-of-

64 views of 26.2 by 16.5 km and 13.7 by 10.3 km with its 18.7 and 36.5 GHz channels for mean
65 resolutions of 21 and 12 km, respectively. On the other hand, SSM/I has integrated field-of-
66 views of 70 by 45 km and 38 by 30 km with its 19.35 and 37.0 GHz channels for mean
67 resolutions of 56 and 33.8 km, respectively. AMSR-E scans conically with a swath width of
68 1450 km at an incidence angle of 55^{o} while SSM/I scans with a swath width of 1390 km at an
69 incidence angle of 53.1^{o}. The wider swath for AMSR has enabled almost complete coverage near
70 the poles where data are usually missing due to satellite inclination. Also, AMSR-E has twelve
71 channels from 6 GHz to 89 GHz, while SSM/I has only 7 channels from 19 GHz to 85 GHz. The
72 lower frequency channels (6.9 and 10.65 GHz) of AMSR-E provide the ability to retrieve Sea
73 Surface Temperature (SST) and Surface Ice Temperature (SIT) that are useful not only as climate
74 data sets but also in removing ambiguities in the retrievals due to atmospheric and surface
75 temperature effects. Furthermore, the higher resolution minimizes the uncertainties associated
76 with the use of mixing algorithms to retrieve geophysical sea ice parameters.
77 The polar regions are expected to provide early signals of a climate change primarily
78 because of the so called "ice-albedo feedback" which is associated with the high reflectivity of ice
79 and snow covered areas compared to ice free areas. Recent reports have indeed shown that the
80 perennial ice cover in the Arctic has been declining at a rapid rate of about 10 % per decade
81 (Comiso, 2002; Stroeve et al., 2004, Comiso, 2006). While this has led to speculations of an ice
82 free Arctic in summer within this century, hemispherical changes including those from seasons
83 other than summer have been more modest at about 2 to 3% per decade (Bjorgo et al., 1997;
84 Parkinson et al., 1999; Serreze, 2000). Moreover, in the Antarctic, the trend is also modest but in
85 the opposite direction (Cavalieri et al., 1997; Zwally et al., 2002). The significance of estimates
86 in the trends, have not been fully evaluated because of unknown uncertainties in the parameters
87 derived form historical satellite data. A key problem is that data from a number of different
88 sensors have to be assembled together to make up the historical time series of satellite data we
89 currently have. There are also mismatches in calibration and resolution and there are no
90 measurements that can be used to assess the true large scale characteristics of the sea ice cover
91 and evaluate the accuracy of existing ice data.
92 The launch of AMSR-E is thus timely in this regard in that the data provide the much
93 needed baseline for evaluating the historical record of satellite ice data including the validity of
94 aforementioned trends. Although the time series of AMSR-E data is still short it can also be used
95 in conjunction with historical data to obtain even more accurate trend values. Analysis of

AMSR-E data benefits from the availability of the Moderate Resolution Imaging Spectroradiometer (MODIS) on board the Aqua satellite which provides concurrent observations of the same surface as AMSR-E at a much higher resolution (250 m) during clear skies conditions. Preliminary studies have shown that ice characterization from AMSR-E agrees favorably with those MODIS data in the visible channels obtained during clear sky conditions (e.g., Comiso, 2004).

2. Consistent Retrieval of Sea Ice Concentrations

The spatial distributions of sea ice in the two hemispheres are quite different in that sea ice is surrounded by continental land masses in the Northern Hemisphere while in the Southern Hemisphere, it is sea ice that surrounds a land mass, which in this case is continental Antarctica (Figure 1). In the winter, the Arctic basin is basically covered by consolidated ice that is more confined, thicker and colder than those in the Antarctic. In the Arctic, a large fraction of the ice floes survives the summer melt and can be as old as 7 years (Colony and Thorndike, 1985), while in the Antarctic, it is rarely the case that an ice floe is older than 2 years, the reason being that the ice that survives the summer melt in the region usually gets flushed out of the original location and to the warmer waters by strong ocean currents (e.g., Weddell gyre) during autumn and winter. Also, the impact of divergence on Antarctic sea ice is stronger than in the Arctic because of the lack of an outer boundary in the former, causing more and larger leads and basically more new ice than in the former.

Sea ice is an inhomogeneous material consisting of ice, brine, air pockets, and other impurities, the relative percentages of which are different depending on formation conditions and history of the ice (Weeks and Ackley, 1986; Tucker et al., 1992; Eicken, 1991). We now know that these inhomogenieties affect the dielectric properties of sea ice in the two regions and hence the emissivity or radiative characteristics (Vant et al., 1974; Grenfell, 1992). Hemispherical differences in environmental conditions thus make the radiative signatures of sea ice in the Arctic generally different from those in the Antarctic. This leads to differences in the brightness temperatures as measured by passive microwave sensors, especially for consolidated ice, making it necessary to use different input data for the sea ice algorithms used to retrieve sea ice parameters in the two hemispheres (Comiso et al., 2003a; Comiso, 2004).

Among the most basic geophysical cryospheric parameters that are derived from passive microwave data is sea ice concentration. Sea ice concentration, C_I, has been defined as the

128 percentage fraction of sea ice within the field of view of the sensor. Such percentage has been
129 calculated using a linear mixing equation (Zwally et al., 1983) given by
130
131 $$T_B = T_I C_I + T_O(1-C_I) \quad (1)$$
132
133 where T_B is the observed brightness temperature while T_I and T_O are the brightness temperature
134 of sea ice and open water, respectively, in the region of observation. The sea ice algorithms are
135 formulated with a goal of estimating T_I and T_O within the satellite footprint as accurately as
136 possible. In the Rayleigh-Jeans' approximation, the brightness temperature of a surface is equal
137 to its effective emissivity multiplied by the physical temperature of the emitting surface. The
138 equation (1) suggests that data from only one channel is required but ability to obtain the
139 appropriate T_I and T_O values would be limited because of known spatial and temporal variability
140 of emissivity and temperature within the ice pack (Comiso, 1983; Parkinson et al., 1987; Comiso,
141 1995). The advent of multichannel systems, such as SMMR, allowed the development of
142 algorithms that circumvents this problem (Cavalieri et al., 1984; Svensen et al., 1984; Swift et al.,
143 1986; Comiso, 1986). Such algorithms have been further refined to take advantage of the added
144 capabilities of the AMSR-E sensor (Markus and Cavalieri, 2000; Comiso et al., 2003). This
145 study makes use of the Bootstrap algorithm, that utilizes the 19 and 37 GHz channels at vertical
146 polarization and the 37 GHz channels at horizontal polarization for both hemispheres, as
147 described in Comiso(2004).
148 Change studies, especially in relation to climate, require as long historical record as
149 possible. Unfortunately, current record on global sea ice cover data has not been that long since
150 such data did not exist until the advent of the satellite era. The era started with the Nimbus-
151 5/Electrically Scanning Microwave Radiometer (ESMR) which was launched in December 1972
152 and was the first microwave imaging (or scanning) system. The sensor is a one-channel system
153 with a peak frequency of about 19 GHz and acquires data at variable incidence angles (since
154 scanning is done cross-track). The more current sensors like SMMR, SSM/I and AMSR-E are
155 conically scanning sensors that acquire data at fixed angles thereby making the latter easier to
156 interpret and to be used in the retrieval of geophysical parameters. The ice concentrations
157 derived from the ESMR sensor are thus not as accurate as those from the other sensors mainly
158 because single channel data do not provide the means to resolve ambiguities associated with the
159 presence of many ice types that have different emissivities. Furthermore, the ESMR data set has

lots of gaps (sometimes several months for each year) because of hardware related problems. While ESMR provided some useful sea ice data during the 1973 to 1976 period, trend studies of the sea ice cover usually starts with the SMMR data and covering the period from November 1978 to the present for optimum accuracy. But even with this restriction, putting together a data set using SMMR, SSM/I and AMSR-E is not trivial because of different attributes and characteristics of the different sensors. As will be discussed, mismatches in the locations of the ice edges can occur because of different resolutions and other factors. There can also be mismatches in ice concentration from different sensors on account of slightly different peak frequencies, different incident angles and different calibration for the different sensors.

The initial step for this study is to create a time series of sea ice data from the different sensors that are as consistent as possible. In particular, we made the brightness temperatures (TBs) for the different sets of channels used to generate the ice concentration maps to match to each other as closely as possible. This in part minimizes effects of inconsistent calibration, incident angle, and peak frequency. This was done by first making SSM/I TBs to be consistent with those of AMSR-E TBs for each set of channels by normalizing the values of the former using parameters derived from linear regression of data from the two sensors during overlap periods. This was followed by making data from the different SSM/I sensors consistent and after that by getting the SMMR TBs consistent with SSM/I TBs. The next step is to use same sea ice concentration algorithm (i.e., the Bootstrap Algorithm as indicate above) for data from all sensors. Although it is the same formulation, the Bootstrap Algorithm will be called ABA when applied to AMSR-E data and SBA when applied to SSM/I data. Finally, the same techniques are used for the land mask, ocean mask, and land/ocean boundary masks as described in Comiso (2004) when generating the ice concentration maps.

To illustrate how well we succeeded with the aforementioned strategy, ice concentration maps from AMSR-E and SSM/I on 15 February 2003 in the Northern Hemisphere and on 15 September 2003 in the Southern Hemisphere are shown in Figure 2. In general, the technique appeared to have worked very well with the resulting daily ice concentration maps from different sensors showing very good agreement during overlapping periods. There are subtle differences especially near the ice margins associated with differences in resolution and antenna patterns of the different sensors but ice concentration values in practically all regions are virtually identical.

191 The good agreement in ice concentration is encouraging since it means that the same features of
192 the ice cover are reproduced by the different sensors. The minor differences, which are mainly
193 confined near the marginal ice zones, are inevitable because of innate differences in resolution,
194 the peak frequencies for the radiometer channels used in the algorithm, the incident angle and the
195 antenna side lobes. To gain insight into these differences, we first examine the procedure for
196 masking open ocean areas which is basically done by setting a threshold below which the data is
197 considered as open ocean. The large contrast of the passive microwave signature of sea ice and
198 open water at some of the channels has enabled estimates of the ice concentration at almost all
199 values except at some low ice concentration values where the signature of open water and ice
200 covered surfaces are virtually identical. Moreover, areas in the open ocean that are under the
201 influence of abnormal weather conditions can have signatures similar to those of ice covered
202 ocean. The use of a combination of 19, 22, and 37 GHz channels for the sensors, however,
203 allows for effective discrimination of open ocean data under unusual conditions as illustrated in
204 the scatter plots in Figure 3. In figures 3a and 3b, we show scatter plot of TB(19,V) versus the
205 difference TB(22,V) – TB(19,V) using SSM/I and AMSR data , respectively, while in figures 3c
206 and 3d, we show the corresponding plots but of TB(19,V) versus TB(37,V). The blue data points
207 in the scatter plot along OW actually represent data from the open ocean at all weather conditions
208 while the black data points are those from ice covered ocean. Open water within the pack is
209 usually relatively calm and provides the lowest emissivity of data points along OW and is
210 therefore represented in the algorithm as a data point close to the label O. In the open ocean the
211 surface gets disrupted occasionally by strong winds and bad weather causing big waves and foam,
212 causing the signature to move to higher values and towards W in the scatter plot, depending on
213 the strength of the disruption. In the algorithm, data points along OW are masked to represent
214 open water only with the red line, representing approximately 10% ice concentration used as the
215 threshold as described in Comiso et al. (2003). To obtain consistent ice extent and ice area from
216 SSM/I and AMSR-E data, it is thus important to have the same threshold for both sensors. The
217 set of data points between O and W which are considered as open water areas and should be
218 separated from the ice covered surfaces with 10% ice concentration and above in the same way.
219 The higher resolution of AMSR provides a better definition of the marginal ice zone and a
220 more precise location of the ice edge as previously indicated by Worby and Comiso (2000). This
221 is clearly illustrated in the plots of brightness temperatures at different frequencies across the
222 marginal ice zone (i.e., 35° W longitude) in the Antarctic for both AMSR and SSM/I (Figure 4).

223 The plots show that the brightness temperatures are relatively low and uniform in the open water
224 (left side) and gradually increase over the marginal ice zone and reached their highest values over
225 the consolidated ice region. Over the marginal ice zone that includes the ice edge, the changes in
226 TBs are coherent and consistent at all AMSR-E frequencies. The TBs are not so consistent for
227 the different SSM/I channels (not shown). The corresponding plots for ice concentration, as
228 shown in Figure 4c, indicate that AMSR-E provides a more defined ice edge than SSM/I with the
229 latter further away from the pack by about 12 km. Such discrepancy makes it almost impossible
230 to get a perfect match in the estimates of ice extent using data from the two sensors as will be
231 discussed later. Similar plots for ice concentration in the Barents Seas in the Northern
232 Hemisphere along the 35 ^{o}E and 45 ^{o}E longitudes (Figures 5a and 5b) show basically the same
233 effect but sometimes, the difference can be more modest. It is apparent that a bias exists, with the
234 SSM/I data showing a location of the ice edge that is further away from the pack than the AMSR-
235 E data. This phenomenon is associated with differences in resolution and side lobes of the
236 antenna. The coarser the resolution is, the more the ice covered areas overlap with the open
237 ocean. The effect of the antenna sidelobe is to cause a smearing at the ice edge since higher
238 brightness temperature is observed as the satellite crosses the ice edge from the pack to the open
239 ocean than vice versa. Such smearing is more pronounced with the SSM/I than the AMSR-E data
240 which has a narrower field-of-view (and higher resolution) than the former.
241
242 **3. Comparison of Sea Ice Extents, Area and Ice Concentration during Overlap Period**
243 The ice parameters derived from satellite ice concentration data that are most relevant to
244 climate change studies are sea ice extent and ice area. Ice extent is defined here as the integrated
245 sum of the areas of data elements (pixels) with at least 15% ice concentration while ice area is the
246 integrated sum of the products of the area of each pixel and the corresponding ice concentration.
247 Ice extent provides information about how far north the ice goes in winter and how far south it
248 retreats towards the continent in the summer while the ice area provides the means to assess the
249 total area actually covered by sea ice, and also the total volume and therefore mass of the ice
250 cover, given the average thickness. In the previous section we discussed the technique we used
251 for obtaining consistent ice concentrations from the various sensors. We now show how
252 consistently we can get the ice extent and ice area from these sensors as well as average ice
253 concentrations during periods of overlap. Figures 7a-7f show distributions of daily average ice
254 extent, ice area and ice concentration over an entire annual cycle using AMSR-E and SSM/I data

255 in 2005 for both Northern and Southern Hemispheres. The plots in Figures 7a and 7b show that
256 the extents derived from SSM/I data (in blue) are consistently higher than those from AMSR-E
257 data (in red) with the difference in winter relatively smaller than those in the summer period. The
258 plots in Figures 7c and 7d show that the ice areas derived from SSM/I are still higher but much
259 more consistent with those derived from AMSR-E data. These results sugest that the mismatch in
260 resolution affects estimates of the extent more than the ice area with the coarser resolution system
261 (i.e., SSM/I) providing the higher extent because of smearing effect as described earlier. The
262 average ice concentrations from AMSR-E (Figures 7e and 7f) are also shown to be consistently
263 higher by about 1 to 2% than that of SSM/I. This in part made the ice area from the two sensors
264 more compatible. The main reason for the difference in extents from the two sensors is that there
265 are more data elements with ice for SSM/I than AMSR-E, mainly because the ice edges in the
266 former extends further beyond the MIZ than the latter, as discussed earlier. These additional data
267 elements have low concentration values the inclusion of which causes the average ice
268 concentration to be lower. The additional low ice concentration data also makes the average ice
269 concentration lower for SSM/I than AMSR. The discrepancy is not so apparent with the ice area
270 because the ice concentrations maps (see Figure 2, for example) basically match each other and
271 the contribution of low concentration pixels at the ice edge is not as significant for ice area as
272 with the ice extent estimates.

273 Similar comparative analysis of ice extents, ice area and ice concentration using data from
274 two SSM/I sensors (i.e., F11 and F13) during the period of overlap from May to September 1995
275 is presented in Figure 8. The plots show very good agreement of data from the two sensors. This
276 is not a surprise since the two sensors have virtually the same attributes. Slight differences in ice
277 concentration estimates occur (e.g., 20 July 1995) but this may be associated with radiometer
278 noise. It should be noted, that the good agreement was obtained after the two sensors were
279 intercalibrated and the TBs were made consistent. Although the resolutions of F11 and F13 are
280 expected to be the same, consistency in the derived ICs is needed to get consistency in the extent
281 and area.

282 During the overlap of SSM/I and SMMR data in mid July to mid-August in 1987 the
283 extents and areas are also in relatively good agreement (Figure 9) during this summer period in
284 the Arctic and the winter period in the Antarctic. It is interesting to note that the agreement was
285 better during August than in July in the Northern Hemisphere but the opposite is true in the
286 Southern Hemisphere. Also, the SSM/I values tend to be higher than those of SMMR in the

Northern Hemisphere in July while the reverse is true in the Southern Hemisphere in August. Furthermore, the differences in the average ice concentrations are larger in the Northern Hemisphere than in the Southern Hemisphere and in July, SSM/I values are higher than those of SMMR while the opposite is true in July of the Southern Hemisphere. Because of these inconsistencies, it is not easy to establish whether there is a bias or not, especially since the overlap period is quite short.

Degradation in the quality of the SMMR data was occurring during this period and it is likely that the SMMR observations were not as accurate as those of SSM/I. An overlap of at least one annual cycle would have been desirable if only to establish that the seasonal differences are similar to those shown in Figure 8. In the time series that requires monthly averages, SMMR data were used to generate monthly data for July 1987 while SSM/I data were used for the August monthly. This procedure appears good for the Antarctic data since there is good consistency of the two sensors in this region in July but such advantage is not apparent the Northern Hemisphere.

It is encouraging that the agreement between AMSR-E and SSM/I ice extents and area data is as good as indicated in the plots despite the vast differences in resolution. The use of ice concentration is expected to take care of the resolution problem but not completely especially in the estimates of ice extent. As indicated earlier, the data with lower resolution will find the ice edge further away from the pack than the one with higher resolution. Although the same algorithm is applied on the two data sets, the fields of view and side lobes of the two sensors are different and hence the observed radiances from the two sensors cannot be identical even if the calibration of each is perfect. Also, the location of the ice margins as observed by the two sensors are not expected to be same. One key reason for this is the differences in revisit time of the two sensors: one (SSM/I) crossing the equatorial line at about 10 am while the other (AMSR-E) at about 1 pm. Since the ice cover is dynamic and the ice edge can easily be altered by winds, the ice edge location can be significantly changed within the three hour difference.

It is apparent that errors (or biases) in ice extent has to be considered when combining data from different sensors with different resolutions. This already assumes that the ice concentrations are derived in a similar fashion and the masking for open water, land and ice/ocean boundaries are similar if not identical. There are also mismatches in the estimates for ice area but they are basically small and negligible.

4.0 Monthly Changes and Interannual Trends in the Sea Ice Extents and Areas

4.1 The Northern Hemisphere

The time series of monthly sea ice extents and areas in the Northern Hemisphere from 1978 to the present, as presented in Figure 10, provides the means to evaluate how the ice cover in the entire Northern Hemisphere has been changing during the satellite era. The variabilities in both extent and area are similar and are dominated by a very large seasonality of the ice cover in the region as has been cited previously (e.g., Parkinson et al., 1987). The ice minimum usually occurs in September while the ice maximum occurs either in February or March. The time series shows data from the different sensors in different colors and show basically a smooth transition from one sensor to the other. Although there is overlap of SMMR and SSM/I data for about a month from mid-July to mid-August 1987, the plot shows averages from SMMR for July 1987 and that for SSM/I for August 1987. The only overlap presented is that of SSM/I and AMSR-E which started in June 2002 and continued through 2006. During overlap period, SSM/I extent and area are slightly higher than those of AMSR-E as expected from previous discussions.

The monthly data show large interannual variability in the peak values, the amplitude and also the minimum values for both extent and area. The patterns are also not so predictable with high values in winter not necessarily leading to high values in the summer (e.g., 1974 and 1990). To assess how the length of the growth period has changed over time, the dates of ice minimum and maximum were identified for each year. The length of growth in our case is defined as the time period between the date of ice minimum in one year to the date of ice maximum the following year and for the period 1979 to 2005 and the results gave an average length of 179 days and a declining trend of about -2.5 days per decade. The minimum and maximum dates changes with time but it appears that the difference changes only by a few days and the length of growth had so far been basically stable. It is also apparent that the peak values have been going down since 2002 while the minimum values have been abnormally low during the same years.

To assess interannual trends in the ice cover, we use monthly anomalies as has been done previously (Parkinson et al., 1999; Zwally et al., 2002) in order to minimize the effect of the large seasonal variations. These anomalies were obtained by subtracting the monthly climatological averages from each monthly average. The climatology for each month is the average of all data for this month from November 1978 to December 2006. The monthly anomalies for the ice extents in the Northern Hemisphere are presented as three different combinations of combining

351 the data in Figure 11, namely: (a) SMMR and SSM/I extents only, (b) SMMR, SSM/I and
352 AMSR-E extents with SSM/I data ending where AMSR-E data starts, and (c) normalized SMMR
353 and SSM/I and original AMSR-E extents. Normalization parameters for the last case are derived
354 from data during SSM/I and AMSR-E overlap and are meant to get the two data sets consistent
355 during the period. The first case provides the data that is currently being utilized for trend studies
356 while the second case make use of AMSR-E data instead of SSM/I when appropriate. The trend
357 values for SMMR and SSM/I data only is -3.39 ± 0.18 % per decade while that for SMMR,
358 SSM/I and AMSR-E data is -3.99 ± 0.20 % per decade. There is a difference of -0.60 % per
359 decade in the trends but this is likely associated with the bias as described earlier, due in part to
360 the difference in resolution between AMSR-E and SSM/I. When the bias is removed through
361 aforementioned renormalization, the trend for a combined SMMR, SSM/I and AMSR-E data is -
362 3.37 which is consistent with that for SSM/I and SMMR data only. Taking advantage of the
363 overlap thus enables the AMSR-E data to be utilized in trend analysis. Since the latter is more
364 accurate, the net error in the trend analysis is going to be less and the importance of AMSR-E
365 data in trend studies will increase with time.
366 The range of variability in the anomalies is about 1 x 10^6 km^2 while that for seasonal ice,
367 as revealed by the monthly averages, is about to 8 x 10^6 km^2. It is also apparent that the
368 variability is significantly less for the period 1996 to 2006. This is intriguing since the slope of
369 the data during the latter period appears different from those of the earlier period. Linear
370 regression using only data from 1996 to 2006 yields a trend of more than -8% per decade, which
371 is more than twice the trend from 1978 to 2006. During the last ten years, many unusual events
372 happened in the Arctic. First, there was a record high ice free region in the Beaufort Sea in 1998
373 (Comiso et al., 2003) which was then the warmest year on record globally over a century (or
374 since temperature sensors started to be used). There was also a record low perennial ice cover in
375 2002 which at the same time became the warmest year on record. The perennial ice cover was a
376 record low again in 2005 which also became the warmest year on record. The intervening
377 periods were low ice years as well including that of 2006. It is possible that the values before
378 1996 are representative of the natural variability of sea ice cover in the Arctic but the changes
379 after that may not be part of the natural variability as previously suggested (Overland, 2005). The
380 Arctic ocean surface is expected to warm up as the perennial ice continues to retreat on account
381 of the so called "ice-albedo feedback," and a warmer ocean would delay the onset of ice growth
382 in the autumn and cause an earlier melt onset, thereby causing a shorter ice season and hence

383 thinner and less extensive ice cover. With additional warming expected from increasing
384 greenhouse gases in the atmosphere the trend is expected to continue in the near future.
385 Similar plots but for the ice area are presented in Figure 12, and it is apparent that the
386 variabilities are similar but the trends are more negative with the corresponding trends for the
387 three cases being -4.01 ± 0.18, -4.38 ± 0.19 and -4.00 ± 0.18 %/decade. The more negative trend
388 for ice area compared to those for ice extent is in part associated with a negative trend in the sea
389 ice concentration during the period. Changes in ice concentration may be caused by changes in
390 wind strength and wind patterns that in turn cause changes in the area affected by divergence. In
391 the summer, it can also be caused by changes in the areal extent of meltponding which causes
392 large errors in the estimate of ice concentration (Comiso and Kwok, 1995).
393 For completeness, regional trends in the ice extent are presented in Figure 13. While
394 overall, the trend for the entire hemisphere is moderate at about -3.4 ± 0.2 %/decade there are
395 regions where significantly higher negative trends are apparent. Among these regions are the
396 Greenland Sea, the Kara/Barents Seas, the Okhotsk Sea, Baffin Bay/Labrador Sea, and the Gulf
397 of St. Lawrence where the trends are -8.0, -7.2, -8.7, -8.6, and -10.7, respectively. In these
398 regions, some cyclical patterns are also evident especially in the first 15 years of data. The only
399 region that show positive trend is the Bering Sea which appears to be growing but at a negligible
400 rate of 1.7 ± 2.0 %/decade. This region is one of the few sea ice covered areas in the Arctic that
401 has exhibited some cooling in the last few decades (Comiso, 2003).
402
403 *4.2 The Southern Hemisphere*
404 Monthly extents and ice areas in the Southern Hemisphere, as derived from SMMR,
405 SSM/I and AMSR data (Figure 14) show an even more seasonal ice cover than that of the
406 Northern Hemisphere. Minimum ice extents and ice areas usually occurs in February while
407 maximum ice extents and ice areas occurs in September. This means that the growth period takes
408 a longer time than the melt period in the Southern Hemisphere (see also, Figure 6). The
409 maximum and minimum extents and areas go though interannual fluctuations but they look
410 relatively stable. However, it appears that since the winter of 2002, the maximum values have
411 been increasing but at the same time, the minimum values have been decreasing. It would be
412 interesting if the subsequent years would follow the same pattern and show some modulation in
413 the ice cover.

414 The monthly ice extent anomalies are again presented for the three cases in the Southern
415 Hemisphere (Figure 14) as in the Northern Hemisphere. It is apparent that there is large
416 fluctuation in the monthly anomalies (of about 2 x 10^6 km^2) from 1978 through 1987 and then a
417 much more moderate variation (of about 1 x 10^6 km^2) from 1987 to 1994 that is followed by a
418 larger fluctuation from 1994 through 2006. The monthly extents (Figure 13) do not show large
419 interannual changes during the 1987 to 1994 period and it is not known why the sea ice cover
420 anomalies would go into such transition from high to low variability and then higher variability in
421 the Southern Ocean. Using SMMR and SSM/I data only, the trend in the hemispheric ice extent
422 is 0.945 ± 0.230 %/decade while with SMMR, SSM/I, and AMSR-E data, the trend is slightly
423 lower at 0.684 ± 0.230 %/decade. The difference is again likely associated with differences in
424 resolution as discussed earlier and if SMMR and SSM/I data are normalized to make them
425 consistent with AMSR-E data, the trend is similar to the first, being 0.94 %/decade. Again, in
426 this way, AMSR-E data can be used in trend analysis in conjunction with historical data.
427 The corresponding monthly anomalies for ice area as presented in Figure 15 show the
428 same variability as the ice extent. However, the trends are much more similar in all three cases
429 the values being 1.72 ± 0.25, 1.77 ± 0.26 and 1.72± 0.25 %/decade. Again, the difference of the
430 first two are minor because the contribution of additional pixels along the ice edge caused by
431 differences in resolution does not affect the estimate of area as much as that of the ice extent.
432 After the application of the normalization factors on the SMMR and SSM/I data, the trend in as
433 indicated in Figure 15c of 1.72%/decade is virtually identical to that of Figure 15a.
434 Except for the summer, the sea ice cover around the Antarctic continent is contiguous and
435 therefore, there is no natural boundary as in the Arctic region. For regional studies, we adapt the
436 same sectors used in Zwally et al. (1983). The monthly anomalies for the entire hemisphere and
437 for the different regions, as presented in Figure 16, have very similar variabilities with the
438 possible exception of those in the Ross Sea Sector. The trends in ice extent for the various
439 regions are all positive except that of the Belingshausen-Amundsen Seas Sector, which has been
440 previously identified by Jacobs and Comiso (1997) as a climatologically anomalous region. The
441 trend in this region is currently -5.7 %/decade but this is compensated by a positive trend of 4.2
442 %/decade in the Ross Sea. Some declines in the Ross Sea ice cover is apparent in recent years
443 but they are more than compensated by increases at the Indian Ocean and the West Pacific Ocean.
444
445 **5. Sensitivity and Error Analysis**

To evaluate quantitatively how errors in the determination of the ice edge affects the estimates for the trends in ice extent and ice area we use the original values of SMMR and SSM/I and added a data element at the ice edge in the AMSR-E data. Since each data element has a grid size of about 25 by 25 km this means having an ice edge about 25 km further away. We also did the same for half a pixel and a quarter of a pixel to assess the effect of an ice edge being 12.5 and 6.25 km further away as well. The results are presented in Figures 17 and 18, respectively, for the Northern Hemisphere and the Southern Hemisphere. In the Northern Hemisphere, the trend in extent ranges in value from -3.03%/decade for a bias of a full pixel to -3.99 % per decade for no bias. Comparing with our previous results, the bias at the ice edge is likely about 14 km. In the Southern Hemisphere, the trend in extent ranges from 2.16% per decade for a one pixel bias to 0.68% per decade for no bias. Comparing with our previous results, this translates a bias at the ice edge of about 6 km. The changes in trend for the areas are much smaller.

6. Discussion and Conclusions

The AMSR-E data provide opportunities to study the sea ice cover at higher accuracy and in greater spatial detail than ever before. The greater spectral range and higher resolution data set will enable more in depth studies of many mesoscale processes that occurs in polynyas, divergence areas and marginal ice zones. Comparative studies shows a good match of high resolution AMSR-E data with those of high resolution satellite data providing confidence that the interpretation of large scale as well as mesoscale features identified in the former are indeed accurate. With only about 5 years of good data available, however, the record length is too short for change studies. Change studies using AMSR-E data can thus be made effectively when it is combined with historical satellite data.

This study shows that during the overlap period from June 2002 to 2006 that the ice concentration maps derived from AMSR-E and SSM/I are virtually identical. The ice extents and ice areas estimated from the two sensors are also in very good agreement and both basically provide the same information about seasonal and interannual variability. The historical data therefore provide a reasonably accurate estimate of the trends in the ice cover. However, there are subtle differences, especially in the characterization of the Marginal Ice Zone and the ice edge. Because of higher resolution, AMSR-E is able to provide more precise locations and more accurate gradients in these regions that that provided by SSM/I. This difference is reflected in the estimates of ice extents with the latter providing slightly higher values on account of coarser

478 resolution. With proper normalization, however, the AMSR-E data can still be combined with
479 the historical satellite data for more accurate determination of trends in ice extent. In the
480 estimates of ice area, AMSR-E and SSM/I data provides almost identical values basically since
481 the ice concentrations generally agree and the effect of additional low concentration ice at the ice
482 edges detected by one but not the other is negligible in this estimate.
483 With the higher resolution and improved accuracy, AMSR-E data provide a good baseline
484 for ice cover studies and to test the estimates in extent and area from other sensors. We show that
485 because of coarser resolution, SSM/I data provides a location of the ice edge that is on the
486 average about 6 to 12 km further away from the ice pack than AMSR-E data. Biases if
487 uncorrected could also contribute to errors in the estimates of trends in extents of as much as
488 0.62%/decade in the Arctic and 0.26%/decade in the Antarctic. The biases in ice area are less
489 with the error in the trend of areas being at 0.30%/decade in the Arctic and 0.05%/decade in the
490 Antarctic.
491 Using data from SMMR, SSM/I and AMSR-E and after correcting for the aforementioned
492 bias, the results of our regression analysis for period from November 1978 to December 2006
493 yielded trends in extent and area of sea ice in the Arctic region are -3.4 ± 0.2 and -4.0 ± 0.2 % per
494 decade, respectively. The corresponding values for the Antarctic region are 0.9 ± 0.2 and 1.7 ±
495 0.3 % per decade. These trends are basically the same as those derived using SMMR and SSM/I
496 data only, but with better accuracy since AMSR-E provides more accurate data. With time, the
497 data from AMSR-E and similar instruments will increase the reliability of the trend values.
498
499 **Acknowledgements:** The authors wish to express gratitude to the excellent programming
500 support provided by Robert Gersten of Adnet, Inc. This research was supported by the
501 Cryospheric Sciences Program of NASA Headquarters.
502
503 **REFERENCES**
504 Bjorgo, E. , O.M. Johannessen, and M.W. Miles, "Analysis of merged SSMR-SSM/I
505 time series of Arctic and Antarctic sea ice parameters 1978-1995," *Geophys. Res.*
506 *Lett.*, Vol. 24, pp. 413-416, 1997.
507 Cavalieri, D.J., P. Gloersen, W.J. Campbell, Determination of sea ice parameters with the
508 Nimbus7 SMMR, J. Geophys Res., 89, 5355-5369, 1984.
509 Cavalieri, D.J., P. Gloersen, C. Parkinson, J. Comiso, and H.J. Zwally, Observed hemispheric

asymmetry in global sea ice changes, *Science, 278*(7), 1104-1106,1997.

Cho, K., N. Sasaki, H. Shimoda, T. Sakata and F. Nishio, Evaluation and improvement of SSM/I sea ice concentration algorithms for the Sea of Okhotsk, J. Remote Sensing of Japan, 16(2), 47-58, 1996.

Colony, R. and A. Thorndike, Sea ice motion as a drunkard's walk, J. Geophys. Res, 90, 965-974, 1985.

Comiso, J. C., A rapidly declining Arctic perennial ice cover, *Geophys Res. Letts., 29(20), 1956, doi:10.1029/2002GL015650,* 2002.

Comiso, J.C., Sea ice algorithm for AMSR-E, *Rivista Italiana di Telerilevamento (Italian Journal of Remote Sensing), 30/31*, 119-130, 2004.

Comiso, J. C., D. J. Cavalieri, and T. Markus, Sea ice concentration, ice temperature, and snow depth, using AMSR-E data, *IEEE TGRS, 41(2),* 243-252, 2003.

Comiso, J.C., and K. Steffen, Studies of Antarctic sea ice concentrations from satellite data and their applications, *J. Geophys. Res., 106*(C12), 31361-31385, 2001.

Comiso, J.C., J. Yang, S. Honjo, and R.A. Krishfield, The detection of change in the Arctic using satellite and buoy Data, *J. Geophys. Res. 108*(C12), 3384, doi:1029-2002jc001247, 2003.

Eicken, H., M.A. Lange, and G.S. Dieckmann, Spatial variability of sea-ice properties in the northwestern Weddell Sea, J. Geophys. Res., 96, 10,603-10,615, 1991

Gloersen P., W. Campbell, D. Cavalieri, J. Comiso, C. Parkinson, H.J. Zwally, Arctic and Antarctic Sea Ice, 1978-1987: Satellite Passive Microwave Observations and Analysis, *NASA Spec. Publ. 511*, 1992.

Grenfell, T.C. 1992.Surface-based passive microwave studies of multiyear ice. *J. Geophys. Res.,* **97**(C3), 3485-3501.

Kumerow, C, On the accuracy of the Eddington approximation for radiative transfer in the microwave frequencies," *J. Geophys. Res*, Vol. 98, pp. 2757- 2765, 1993.

Matzler, C., R. O. Ramseier, and E. Svendsen, "Polarization effects in sea ice signatures," *IEEE J. Oceanic Engineering*, Vol. OE-9, pp. 333-338, 1984.

Overland, J.E., The Arctic climate paradox: The recent decrease of the Arctic Oscillation, Geophy. Res. Letters, 32, L06701, doi:10.1029/2004GL021752, 2005.

Parkinson, C.L., D.J Cavalieri, P. Gloersen, H.J. Zwally, and J.C. Comiso, Arctic sea ice extents, areas, and trends, 1978-1996, *J. Geophys. Res., 104*(C9), 20837-20856, 1999.

Parkinson, C. L., J. C. Comiso, H. J. Zwally, D. J. Cavalieri, P. Gloersen, and W. J. Campbell,

542 Arctic Sea Ice 1973-1976 from Satellite Passive Microwave Observations, *NASA Spec. Publ.*
543 *489*, 1987.
544 Serreze, M.C., and Co-authors, Observational evidence of recent chang in the northern high-
545 latitude environment, *Climatic Change, 46*, 159-207, 2000.
546 Steffen, K., D. J. Cavalieri, J. C. Comiso, K. St. Germain, P. Gloersen, J. Key, and I. Rubinstein,
547 "The estimation of geophysical parameters using Passive Microwave Algorithms," Chapter 10,
548 *Microwave Remote Sensing of Sea Ice,* (ed. by Frank Carsey), American Geophysical Union,
549 Washington, D.C., 201-231, 1992.
550 Stroeve, J.C., M.C., Serreze, F. Fetterer, T. Arbetter, M. Meier, J. Maslanik and K. Knowles,
551 Tracking the Arctic's shrinking ice cover: Another extreme September minimum in 2004,
552 *Geophys. Res. Lett. 32*, doi:10.1029/2004GL021810, 2004.
553 Svendsen, E., C. Matzler, T.C. Grenfell, "A model for retrieving total sea ice
554 concentration from a spaceborne dual-plarized passive microwave instrument
555 operating near 90 GHz," *Int. J. Rem. Sens.*, Vol. 8, pp. 1479-1487, 1987.
556 Swift, C.T., L.S. Fedor, and R.O. Ramseier, An algorithm to measure sea ice concentration with
557 microwave radiometers, J. Geophys. Res., 90(C1), 1087-1099, 1985.
558 Tucker, W.B., D.K. Perovich, and A.J. Gow, "Physical properties of sea ice relevant to remote
559 sensing," Chapter 2, *Microwave Remote Sensing of Sea Ice*, (ed. by Frank Carsey), American
560 Geophysical Union, Washington, D.C., 9-28, 1992.
561 Vant, M.R., R.B. Gray, R.O. Ramseier, and V. Makios. 1974. Dielectric properties of fresh and
562 sea ice at 10 and 35 GHz, *J. Applied Physics, 45(11)*, 4712-4717.
563 Weeks, W.F., and S. F. Ackley, The growth, structure and properties of sea ice, *The Geophysics*
564 *of Sea Ice,* edited by N. Unterstiener, pp. 9-164, *NATO ASI Ser.B*, vol. 146, Plenum, New
565 York, 1986.
566 Worby, A. P., and J. C. Comiso, Studies of Antarctic sea ice edge and ice extent from satellite
567 and ship observations, *Remote Sensing of the Environment, 92*(1), 98-111, 2004.
568 Zwally, H.J., J.C. Comiso, C. Parkinson, D. Cavalieri, P. Gloersen, Variability of the
569 Antarctic sea ice cover, *J. Geophys. Res.* 107(C5), 1029-1047, 2002.
570 Zwally, H. J., J. C. Comiso, C. L. Parkinson, W. J. Campbell, F. D. Carsey, and P. Gloersen,
571 Antarctic Sea Ice 1973-1976 from Satellite Passive Microwave Observations, *NASA Spec.*
572 *Publ. 459*, 1983.
573

Figure Captions:

Figure 1. Location map for (a) the Northern Hemisphere; and (b) the Southern Hemisphere. The two shades of gray correspond to the climatological average of the location of the ice cover during minimum and maximum extent.

Figure 2. Daily ice concentration maps during winter in the (a) Northern Hemisphere using AMSR-E data; (b) Northern Hemisphere using SSM/I data; (c) Southern Hemisphere using AMSR-E data; and (d) Southern Hemisphere using SSM/I data.

Figure 3. Scatter plots of TB(V19, V) versus TB(22, V) - TB(19, V) for (a) SSM/I and (b) AMSR-E data. Also, scatter plots of TB(19,V) versus TB(37,V) for (c) SSM/I and (d) AMSR-E data.

Figure 4. Transects along the ice edges of brightness temperatures using AMSR-E (a) vertically polarized and (b) horizontally polarized data and (c) comparison of ice edges as inferred from ice concentration values of AMSR-E and SSM/I.

Figure 5. Ice concentrations along the ice edge in the Barents Sea at (a) 35 ^{o}E and (b) 45 ^{o}E.

Figure 6. Daily ice extents (a &b), ice area (c & d), and ice concentration (e & f) during a period of SSM/I and AMSR-E overlap (2005) in the Northern and Southern Hemispheres

Figure 7. Daily ice extent (a &b), ice area (c & d), and ice concentration (e & f) during a period of SSM/I (F11) and SSM1(F13) overlap (May to September 1995) in the Northern and Southern Hemispheres.

Figure 8. Daily extent (a &b), ice area (c & d), and ice concentration (e & f) during a period of SMMR and SSM/I operlap in the Northern and Southern Hemispheres (July to August 1987).

Figure 9. Monthly extent and area from 1978 to 2006 in the Northern Hemisphere using SMMR, SSM/I and AMSR-E data time series data.

Figure 10. Monthly anomaly and trend in extents from 1978 to the present in the Northern Hemisphere using (a) original SMMR and SSM/I data; (b) original SMMR, SSM/I (up to May 2002) and AMSR-E data (June 2002 to 2006); and (c) normalized SMMR and SSM/I data and original AMSR-E data.

Figure 11. Monthly anomaly and trend in ice area from 1978 to the present in the Northern Hemisphere using (a) original SMMR and SSM/I data; (b) original SMMR, SSM/I (up to May

605 2002) and AMSR-E (June 2002 to 2006) data; and (c) normalized SMMR and SSM/I data and
606 original AMSR-E data.
607 Figure 12. Monthly anomalies of ice extent in the (a) Northern Hemisphere and in the following
608 regional sectors: (b) Arctic Ocean; (c) Greenland Sea; (d) Kara/Barents Sea, (e) Bering Sea; (f)
609 Okhotsk/Japan Seas; (g) Canadian Archipelago; (h) Baffin Bay/Labrador Sea; (i) Hudson Bay;
610 and (j) Gulf of St. Lawrence.
611 Figure 13. Monthly extent and area from 1978 to the present in the Southern Hemisphere using
612 SMMR SSM/I and AMSR-E data
613 Figure 14. Monthly anomaly and trend in extents from 1978 to the present in the Southern
614 Hemisphere using (a) original SMMR and SSM/I data; (b) original SMMR, SSM/I (up to May
615 2002) and AMSR-E (from June 2002 to 2006) data; and (c) normalized SMMR and SSM/I data
616 and original AMSR-E data.
617 Figure 15. Monthly anomaly and trend in ice area from 1978 to the present in the Southern
618 Hemisphere using (a) original SMMR and SSM/I data; (b) original SMMR, SSM/I and AMSR-E
619 data; and (c) normalized SMMR and SSM/I data and original AMSR-E data.
620 Figure 16. Monthly anomalies of ice extent in the (a) Southern Hemisphere and in the following
621 regional sectors: (b)Weddell Sea; (c) Indian Ocean; (d) West Pacific Ocean; (e) Ross Sea; (f)
622 Bellingshausen/Amundsen Seas.
623 Figure 17. Sensitivity of trends to (a) ice extent and (b) ice area with adjustments of AMSR-E
624 data by making the ice edge 6.25, 12.5, and 25 km further away from the ice pack in the Northern
625 Hemisphere during an entire ice season.
626 Figure 18. Sensitivity of trends to (a) ice extent and (b) ice area with adjustments of AMSR-E
627 data by making the ice edge 6.25, 12.5, and 25 km further away from the ice pack in the Southern
628 Hemisphere during an entire ice season.
629

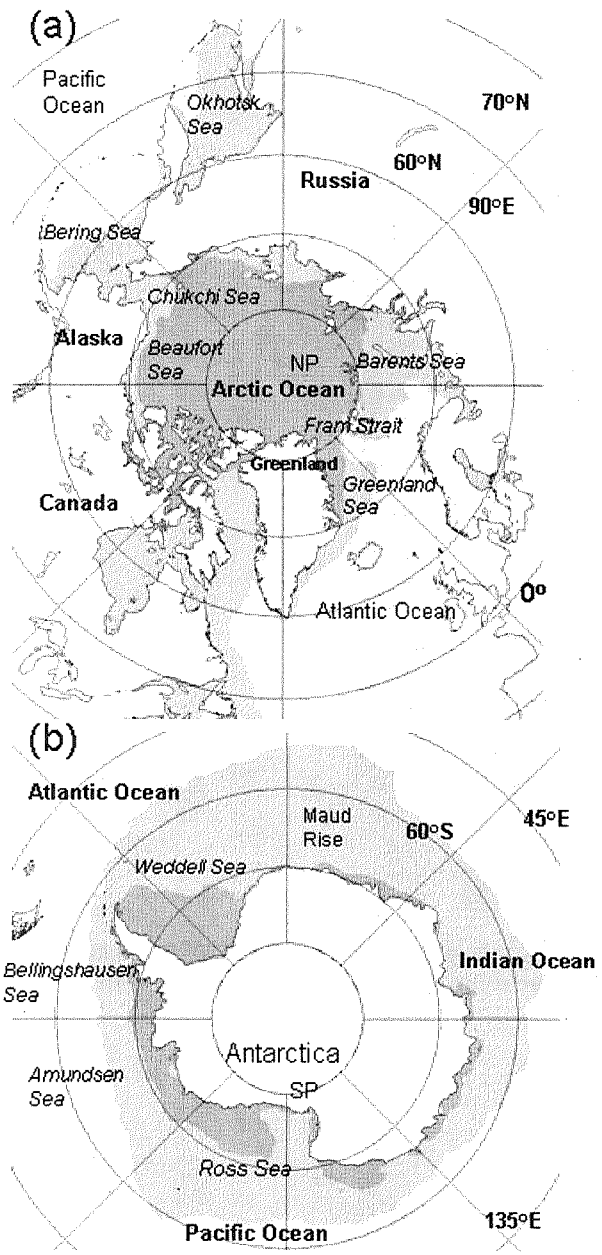

630
631 Figure 1. Location map for (a) the Northern Hemisphere; and (b) the Southern Hemisphere. The two shades of gray
632 correspond to the climatological average of the location of the ice cover during minimum and maximum extent.

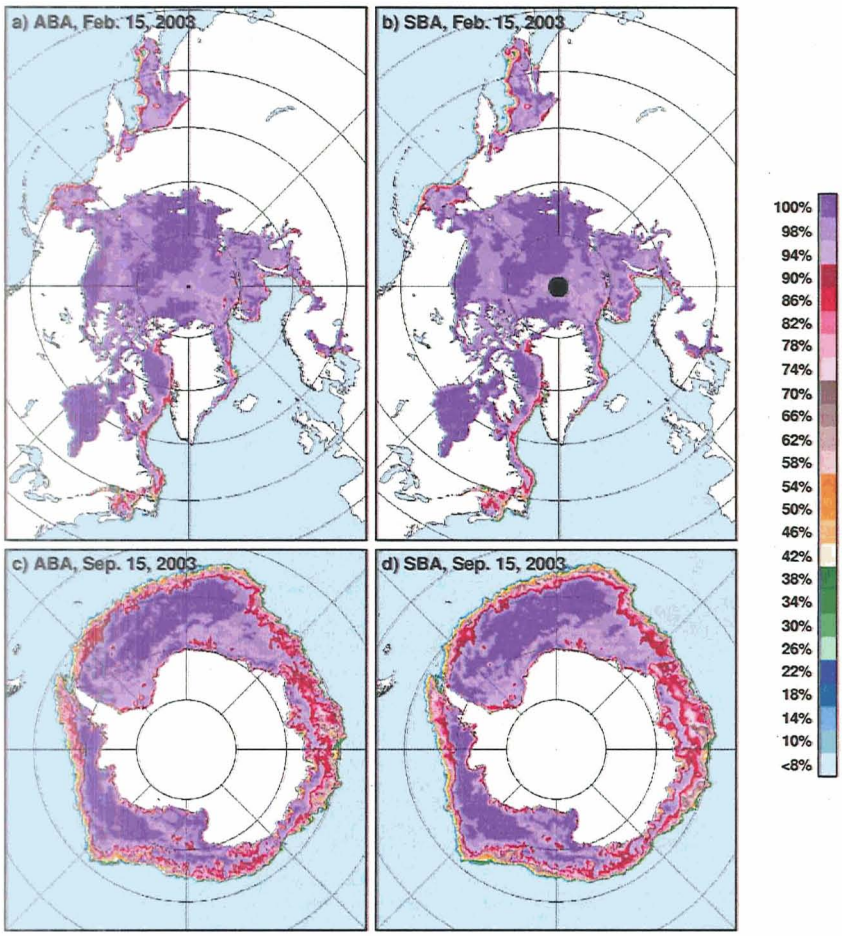

Figure 2. Daily ice concentration maps during winter in the (a) Northern Hemisphere using AMSR-E data; (b) Northern Hemisphere using SSM/I data; (c) Southern Hemisphere using AMSR-E data; and (d) Southern Hemisphere using SSM/I data.

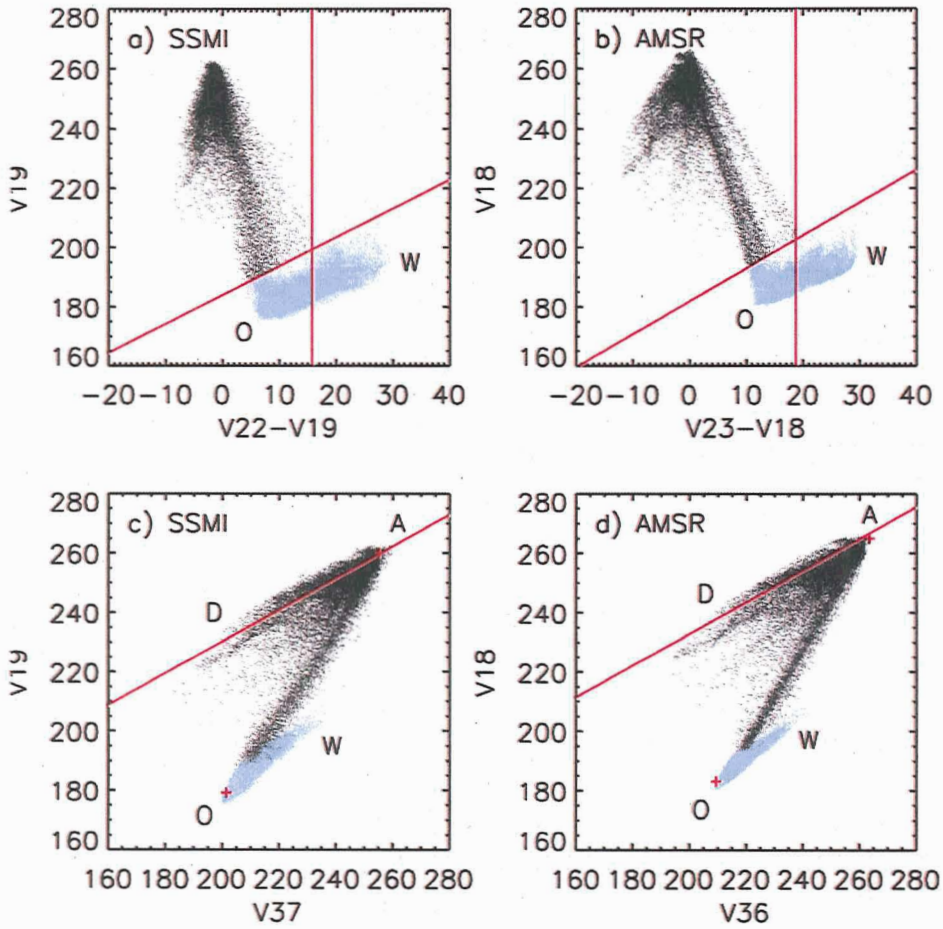

Figure 3. Scatter plots of TB(V19, V) versus TB(22, V) - TB(19, V) for (a) SSM/I and (b) AMSR-E data. Also, scatter plots of TB(19,V) versus TB(37,V) for (c) SSM/I and (d) AMSR-E data.

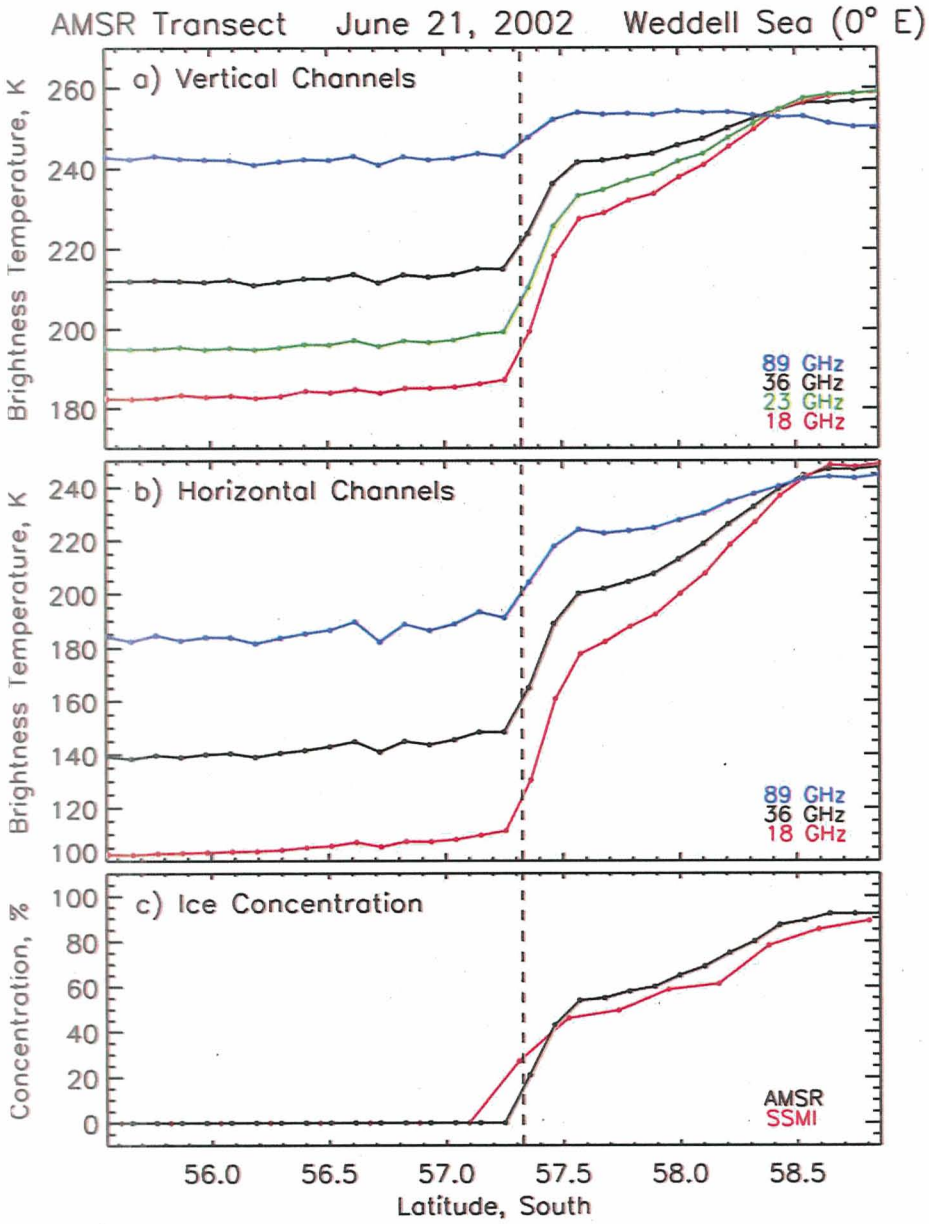

Figure 4. Transects along the ice edge of brightness temperatures using AMSR-E (a) vertically polarized and (b) horizontally polarized data and (c) comparison of ice edges as inferred from ice concentration values of AMSR-E and SSM/I.

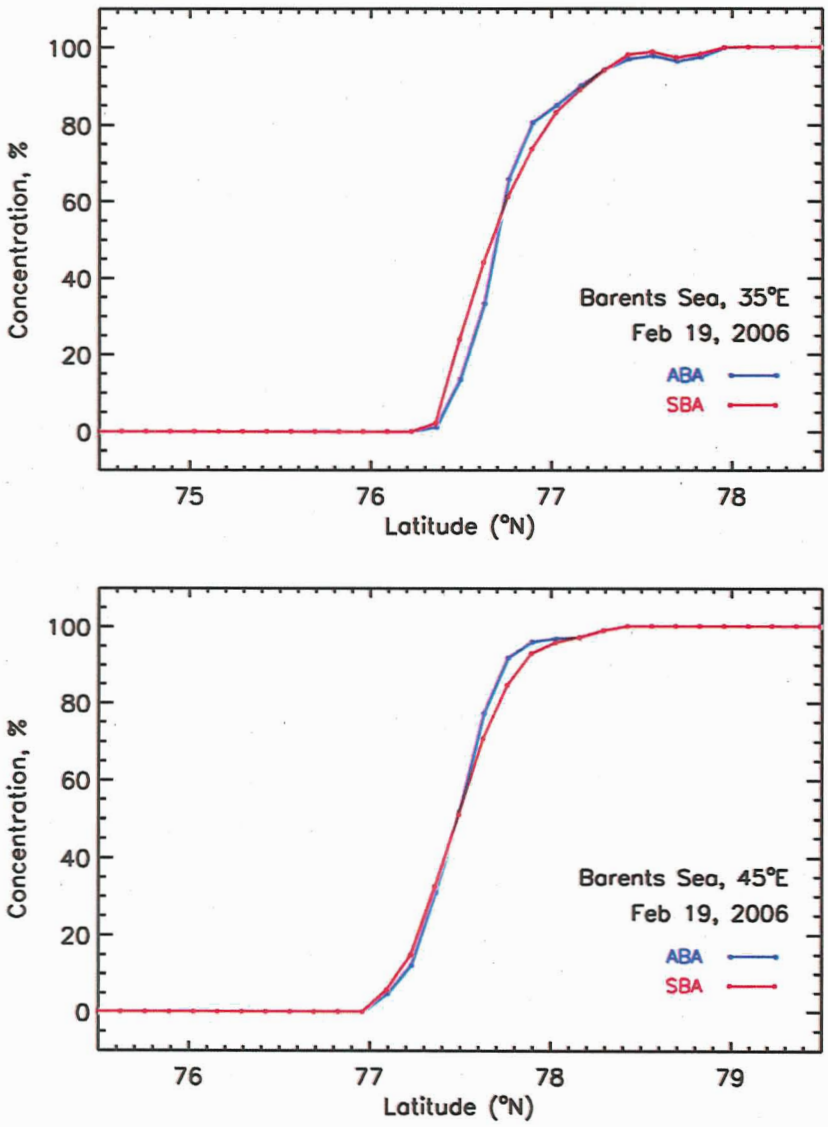

652

653 Figure 5. Ice concentrations along the ice edge in the Barents Sea at (a) 35 °E and (b) 45 °E.
654

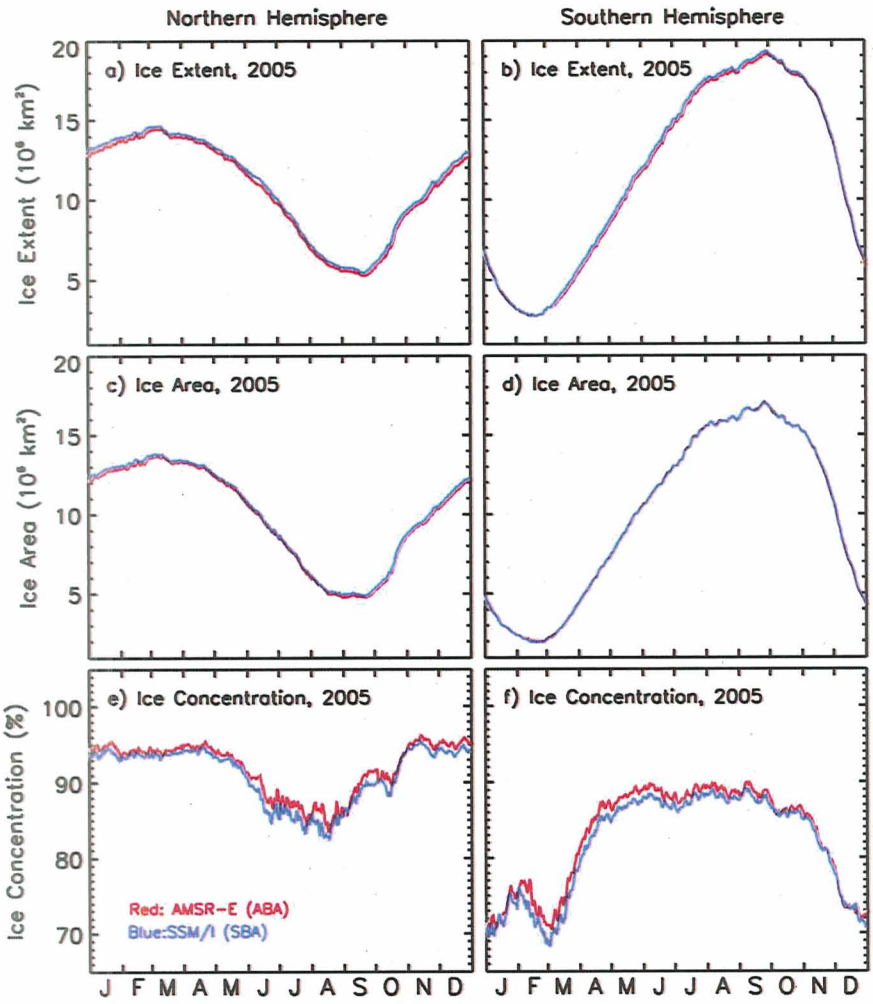

Figure 6. Daily ice extents (a &b), ice area (c & d), and ice concentration (e & f) during a period of SSM/I and AMSR-E overlap (2005) in the Northern and Southern Hemispheres

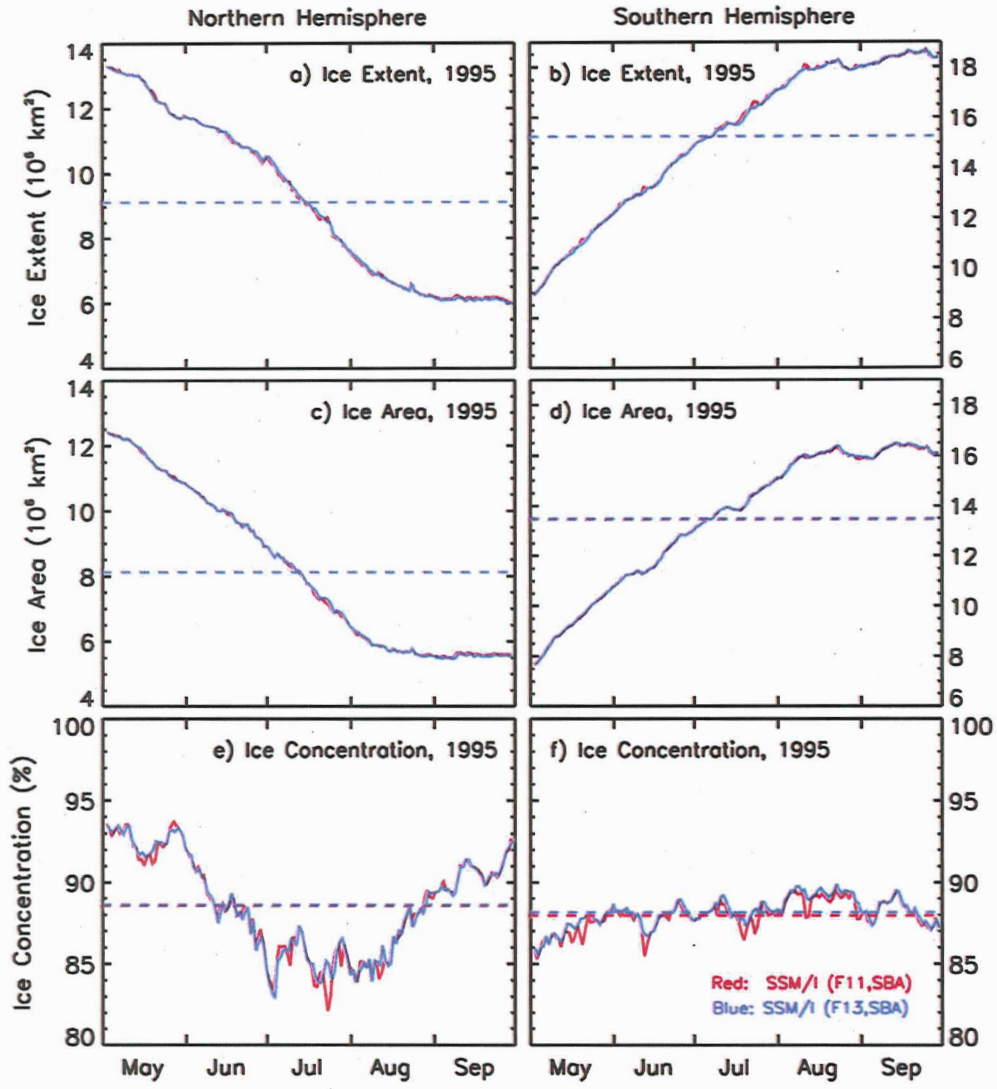

Figure 7. Daily ice extent (a &b), ice area (c & d), and ice concentration (e & f) during a period of SSM/I (F11) and SSM1(F13) overlap (May to September 1995) in the Northern and Southern Hemispheres.

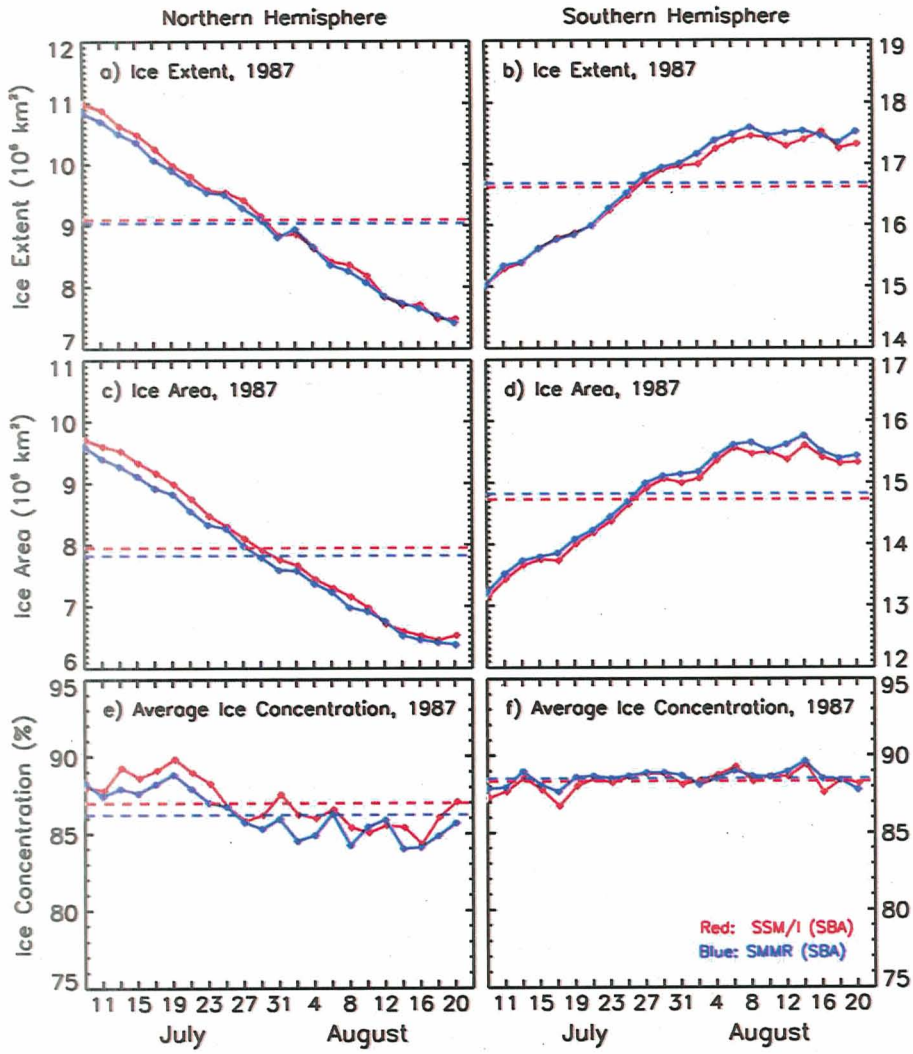

Figure 8. Daily extent (a &b), ice area (c & d), and ice concentration (e & f) during a period of SMMR and SSM/I operlap in the Northern and Southern Hemispheres (July to August 1987).

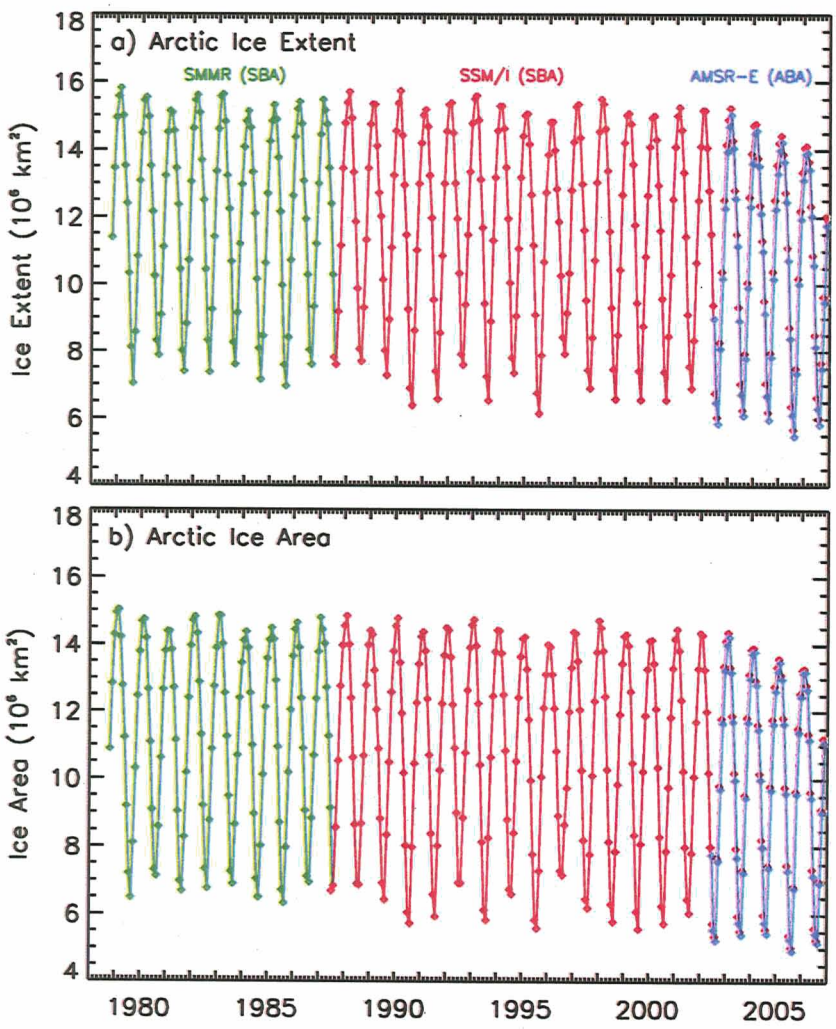

Figure 9. Monthly extent and area from 1978 to 2006 in the Northern Hemisphere using SMMR, SSM/I and AMSR-E data time series data.

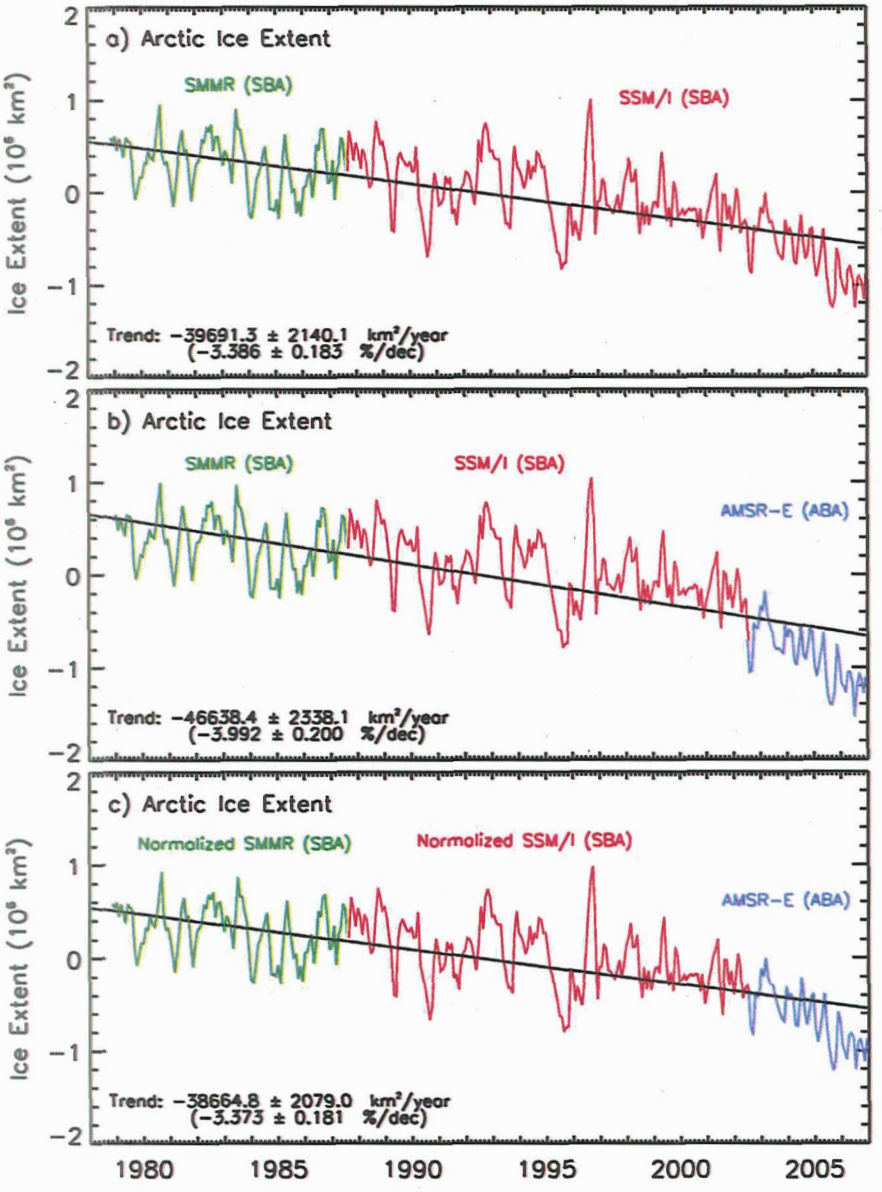

Figure 10. Monthly anomaly and trend in extents from 1978 to the present in the Northern Hemisphere using (a) original SMMR and SSM/I data; (b) original SMMR, SSM/I (up to May 2002) and AMSR-E data (June 2002 to 2006); and (c) normalized SMMR and SSM/I data and original AMSR-E data.

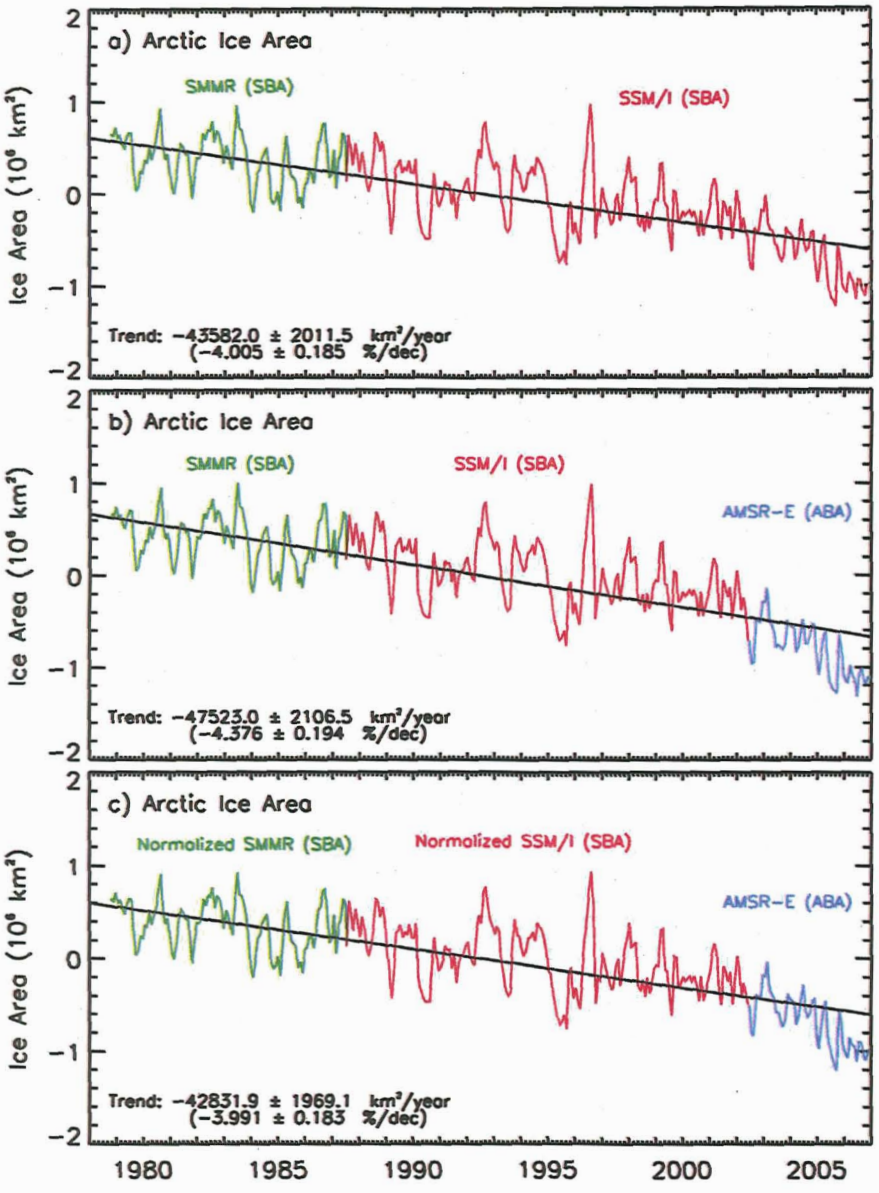

Figure 11. Monthly anomaly and trend in ice area from 1978 to the present in the Northern Hemisphere using (a) original SMMR and SSM/I data; (b) original SMMR, SSM/I (up to May 2002) and AMSR-E (June 2002 to 2006) data; and (c) normalized SMMR and SSM/I data and original AMSR-E data.

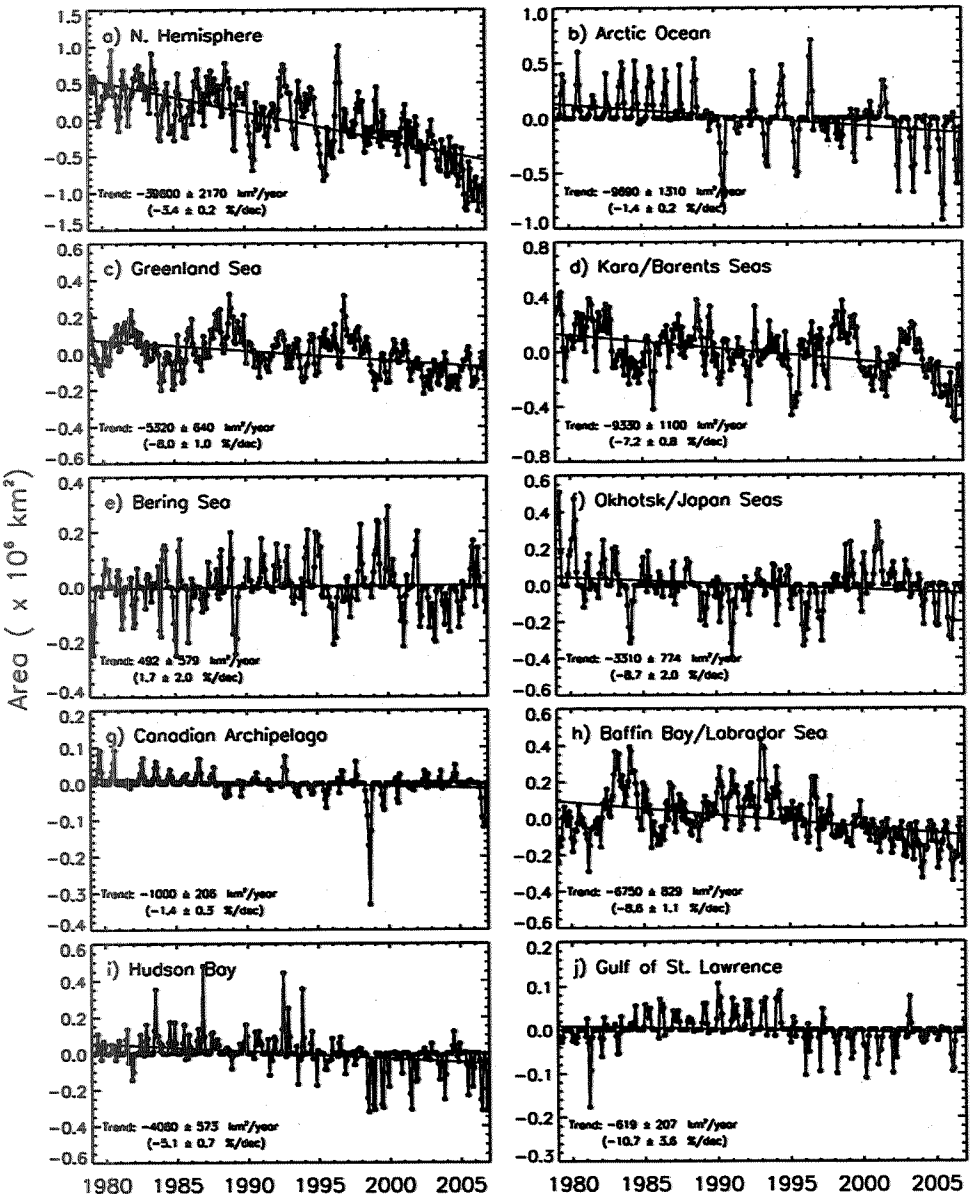

Figure 12. Monthly anomalies of ice extent in the (a) Northern Hemisphere and in the following regional sectors: (b) Arctic Ocean; (c) Greenland Sea; (d) Kara/Barents Sea, (e) Bering Sea; (f) Okhotsk/Japan Seas; (g) Canadian Archipelago; (h) Baffin Bay/Labrador Sea; (i) Hudson Bay; and (j) Gulf of St. Lawrence.

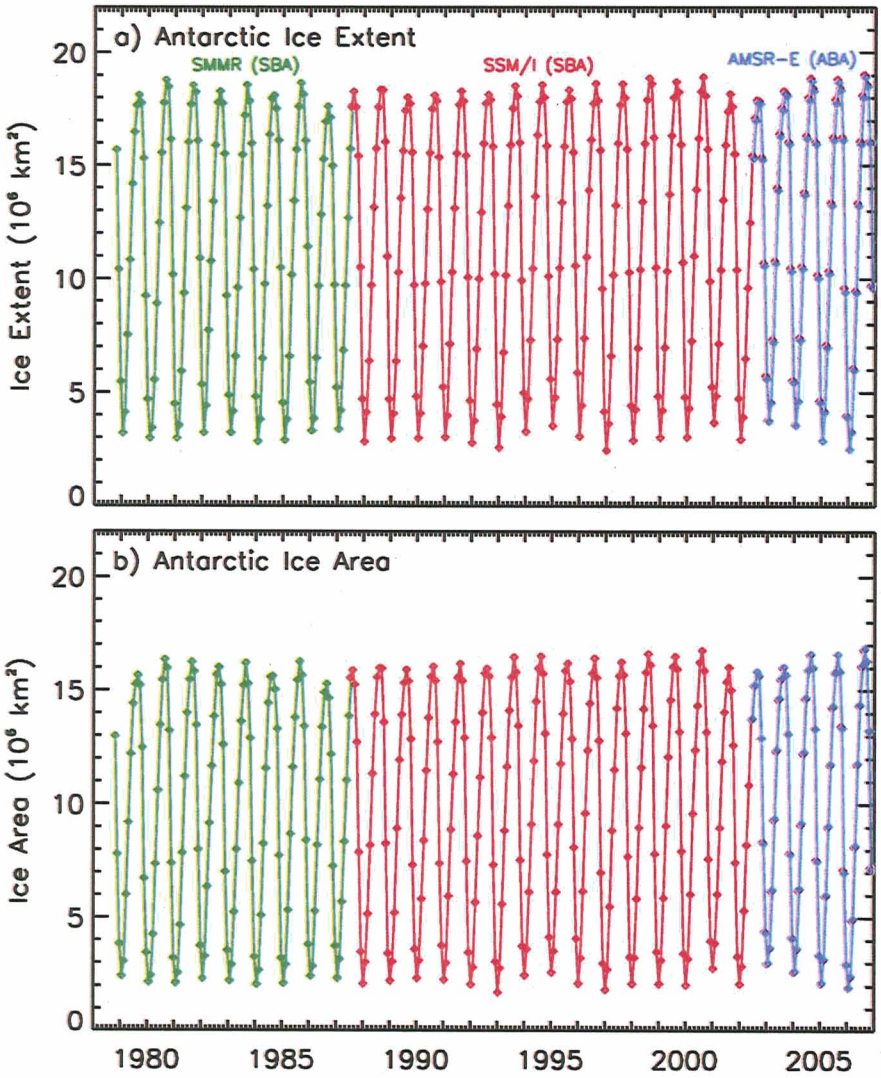

Figure 13. Monthly extent and area from 1978 to the present in the Southern Hemisphere using SMMR SSM/I and AMSR-E data

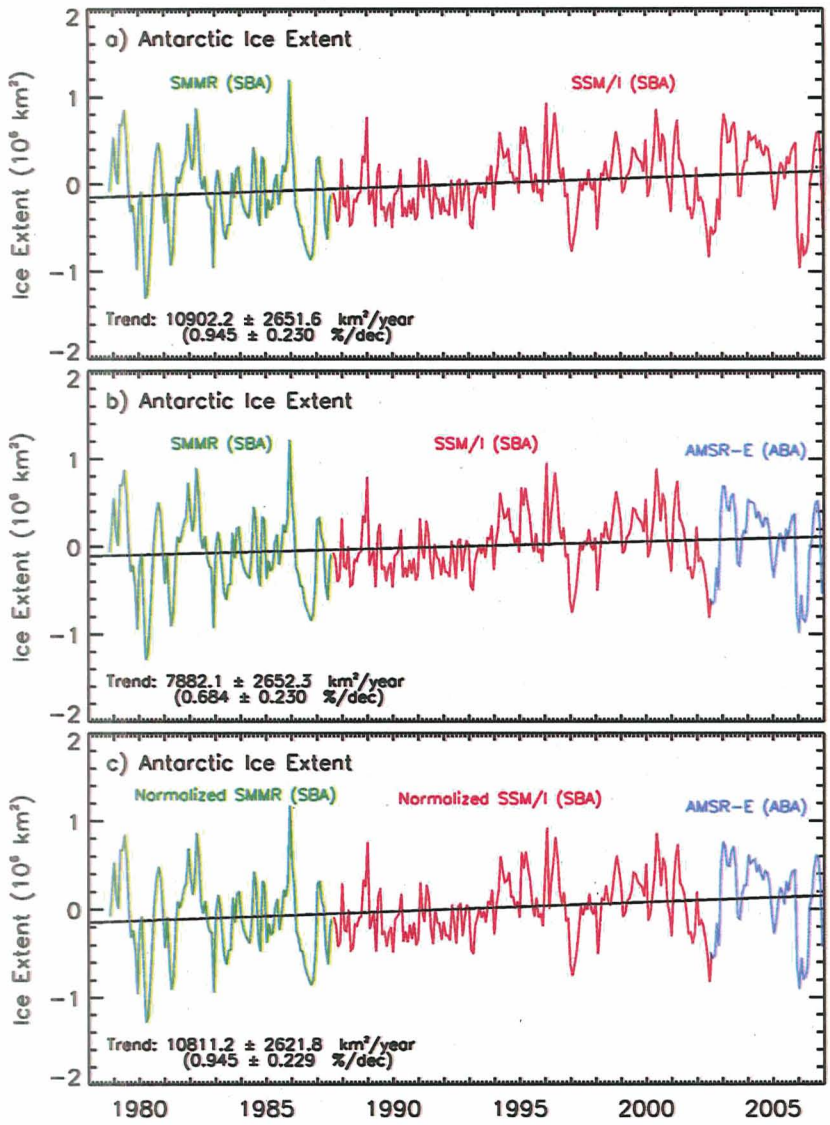

Figure 14. Monthly anomaly and trend in extents from 1978 to the present in the Southern Hemisphere using (a) original SMMR and SSM/I data; (b) original SMMR, SSM/I (up to May 2002) and AMSR-E (from June 2002 to 2006) data; and (c) normalized SMMR and SSM/I data and original AMSR-E data.

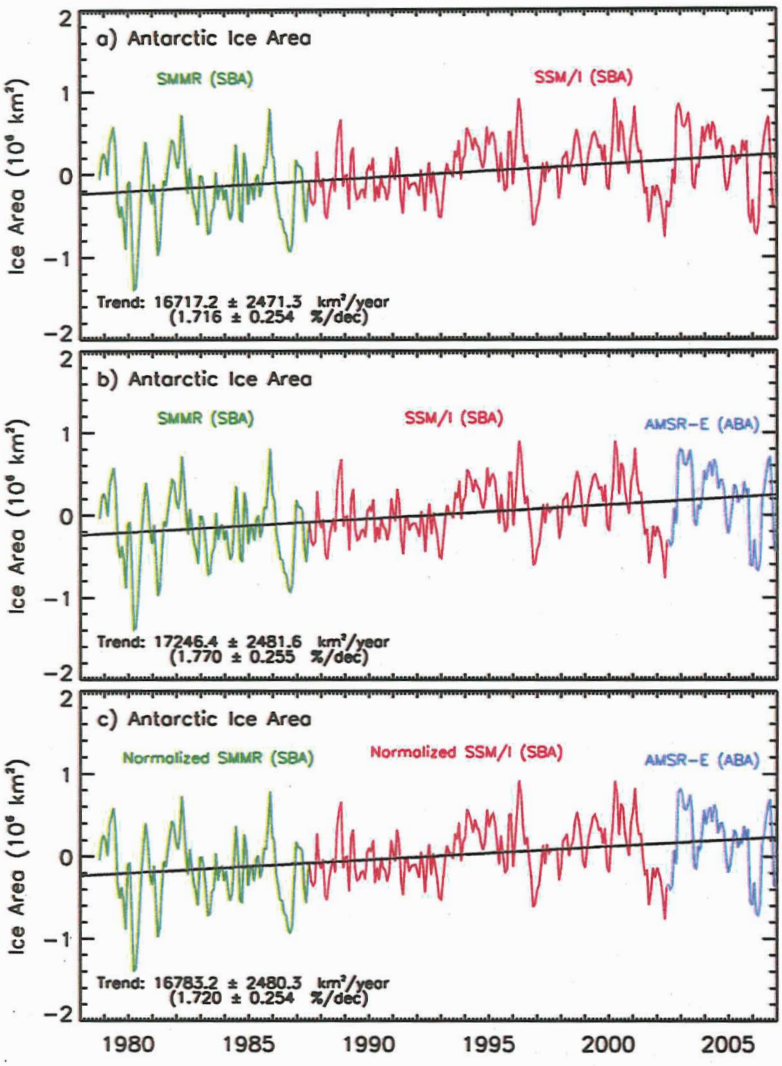

Figure 15. Monthly anomaly and trend in ice area from 1978 to the present in the Southern Hemisphere using (a) original SMMR and SSM/I data; (b) original SMMR, SSM/I and AMSR-E data; and (c) normalized SMMR and SSM/I data and original AMSR-E data.

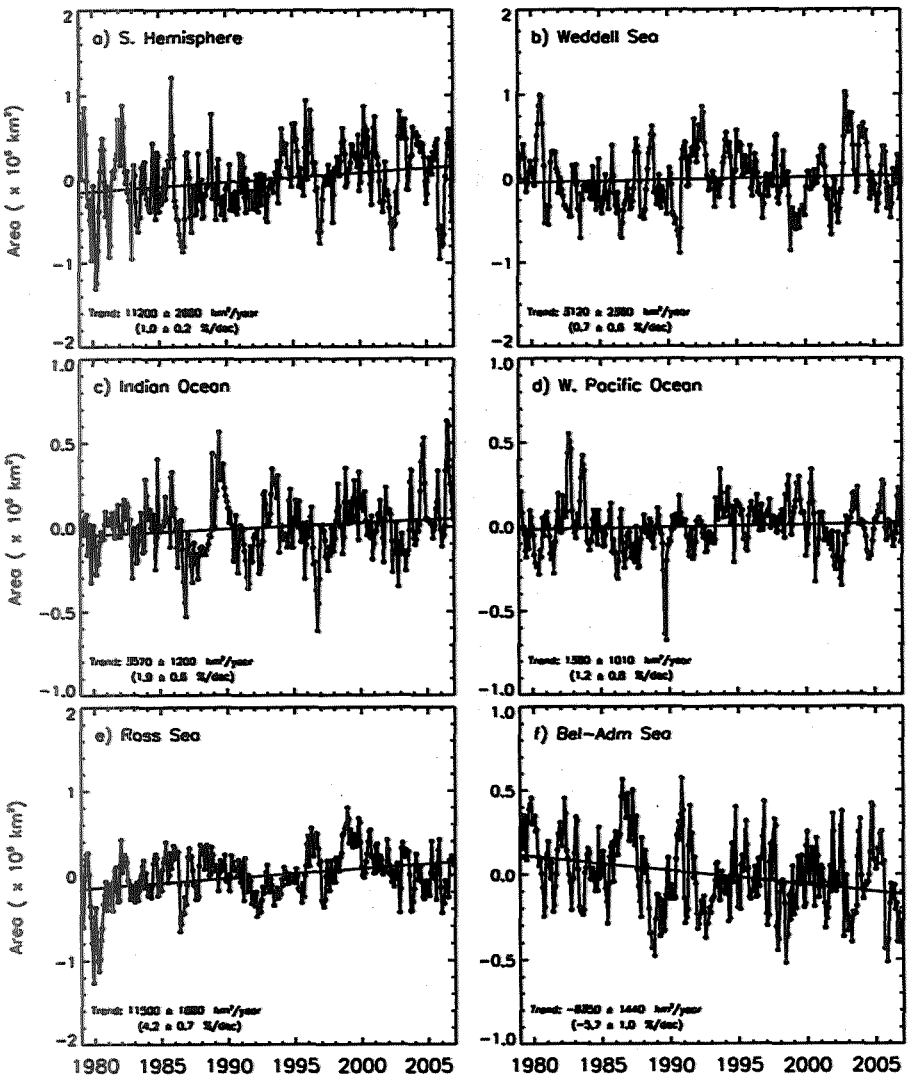

Figure 16. Monthly anomalies of ice extent in the (a) Southern Hemisphere and in the following regional sectors: (b)Weddell Sea; (c) Indian Ocean; (d) West Pacific Ocean; (e) Ross Sea; (f) Bellingshausen/Amundsen Seas.

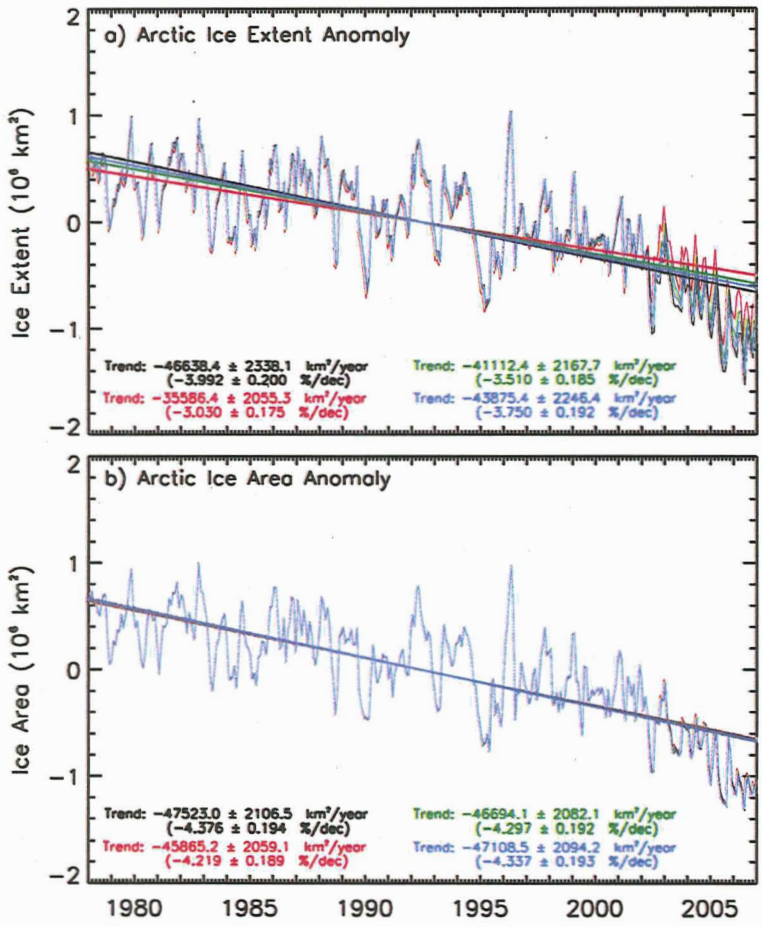

Figure 17. Sensitivity of trends to (a) ice extent and (b) ice area with adjustments of AMSR-E data by making the ice edge 6.25, 12.5, and 25 km further away from the ice pack in the Northern Hemisphere during an entire ice season.

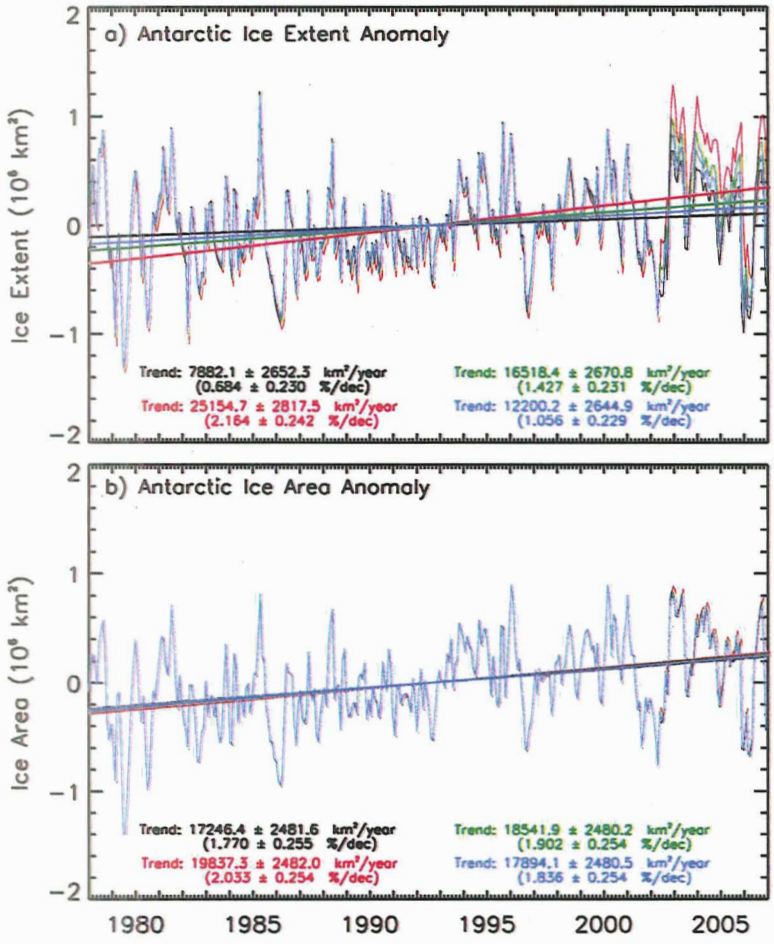

Figure 18. Sensitivity of trends to (a) ice extent and (b) ice area with adjustments of AMSR-E data by making the ice edge 6.25, 12.5, and 25 km further away from the ice pack in the Southern Hemisphere during an entire ice season.